AD-A168 691 STUDY OF VUV GENERATION BY COHERENT RESONANT FREQUENCY MIXING IN METAL VA (U) NORTH TEXAS STATE UNIV DENTON CENTER FOR APPLIED QUANTUM ELEC J DIELS 24 APR 86 1/1

UNCLASSIFIED AFOSR-TR-86-0303 AFOSR-82-0332 F/G 7/4 NL

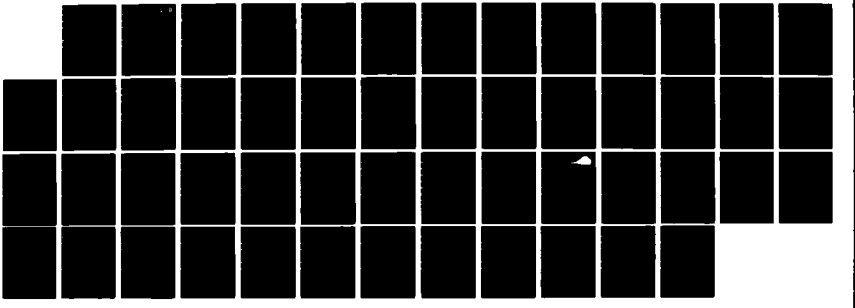

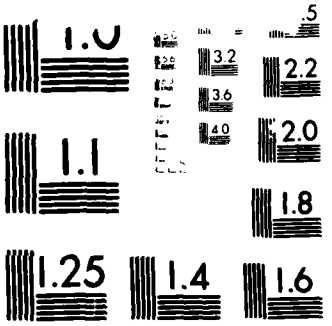
1.0
1.1
1.25
1.4
1.6
1.8
2.0
2.2
3.2
3.6
4.0
.5

SECURITY CLASSIFICATION OF THIS PAGE

AD-A168 691

DOCUMENTATION PAGE

1a. REPORT SECURITY CLASSIFICATION: Unclassified	1b. RESTRICTIVE MARKINGS: None
2a. SECURITY CLASSIFICATION AUTHORITY: N/A	3. DISTRIBUTION/AVAILABILITY OF REPORT: Approved for public release; distribution unlimited.
2b. DECLASSIFICATION/DOWNGRADING SCHEDULE: N/A	
4. PERFORMING ORGANIZATION REPORT NUMBER(S): AFOSR-82-0332	5. MONITORING ORGANIZATION REPORT NUMBER(S): AFOSR-TR- 86-0613
6a. NAME OF PERFORMING ORGANIZATION: North Texas State University	6b. OFFICE SYMBOL (If applicable): N/A
6c. ADDRESS (City, State and ZIP Code): Department of Physics, P.O. Box 5368, Denton, TX 76203	7a. NAME OF MONITORING ORGANIZATION: AFOSR
	7b. ADDRESS (City, State and ZIP Code): Bldg 410, Bolling AFB DC 20332-6448
8a. NAME OF FUNDING/SPONSORING ORGANIZATION: AFOSR	8b. OFFICE SYMBOL (If applicable): N/A
8c. ADDRESS (City, State and ZIP Code): Bolling Air Force Base, Washington, DC 20332	9. PROCUREMENT INSTRUMENT IDENTIFICATION NUMBER: AFOSR-82-0332
	10. SOURCE OF FUNDING NOS.

PROGRAM ELEMENT NO	PROJECT NO	TASK NO	WORK UNIT NO
61102F	2301	A1	N/A

11. TITLE (Include Security Classification): Study of VUV Generation by Coherent Resonant Frequency Mixing in Metal Vapors

12. PERSONAL AUTHOR(S): Dr. Jean-Claude Diels

13a. TYPE OF REPORT	13b. TIME COVERED	14. DATE OF REPORT (Yr., Mo., Day)	15. PAGE COUNT
Final	FROM 10/1/82 TO 10/31/84	1986, 4, 24	50

16. SUPPLEMENTARY NOTATION: N/A

17. COSATI CODES			18. SUBJECT TERMS (Continue on reverse if necessary and identify by block number)
FIELD	GROUP	SUB GR	

19. ABSTRACT (Continue on reverse if necessary and identify by block number)

The properties of multiphoton resonances (two, four or more) are exploited to enhance up-frequency conversion rates. Simultaneously, the property of reversibility of coherent interaction is used to minimize the resonant losses (two-photon, four-photon absorption). A source of tunable, near bandwidth limited pulses, of more than a millijoule energy per pulse has been developed. A new scheme of computer controlled data acquisition system made it possible to analyze, for the first time, the temporal coherence properties of the amplified pulses (at a rate of 20 pps). The method of interferometric autocorrelation has been applied to the study of multi-photon coherences, leading to the first measurement of the phase angle of the third order susceptibility. Experimental demonstration of coherent enhancement of harmonic generation was made. A conversion efficiency of 1% was achieved for third harmonic generation in lithium vapor, which is the maximum efficiency predicted by the theory for this system.

20. DISTRIBUTION/AVAILABILITY OF ABSTRACT	21. ABSTRACT SECURITY CLASSIFICATION
UNCLASSIFIED/UNLIMITED ☒ SAME AS RPT ☐ DTIC USERS ☐	Unclassified

22a. NAME OF RESPONSIBLE INDIVIDUAL	22b. TELEPHONE NUMBER (Include Area Code)	22c. OFFICE SYMBOL
Dr. Schlossberg ~~Jean-Claude Diels~~	(214) 767-4906	~~N/A~~ NP

DD FORM 1473, 83 APR — EDITION OF 1 JAN 73 IS OBSOLETE

UNCLASSIFIED
SECURITY CLASSIFICATION OF THIS PAGE

Report AFOSR-82-0332

STUDY OF VUV GENERATION BY COHERENT RESONANT FREQUENCY MIXING IN METAL VAPORS

Jean-Claude Diels
Center for Applied Quantum Electronics
Department of Physics, P. O. Box 5368
North Texas State University
Denton, Texas 76203

April 20, 1986

Final Report for Period 1st October 1982 - 31st October 1984

Prepared for:
Air Force Office of Scientific Research
Bolling Air Force Base
Washington, D. C. 20332

TABLE OF CONTENT

I General Objectives.....1

II Basic Approach.....2

III Overview of the systems under investigation.....3

IV Coherent interactions in lithium vapor

IV.1. The laser oscillator-amplifier system.....5

IV.2. The lithium-magnesium heat pipe.....8

IV.3. The data acquisition system.....9

IV.4. Nonlinear transmission.....12

IV.5. Data on nonlinear transmission and harmonic generation.....14

IV.6. Phase dependence.....16

IV.7. Phase matching.....18

IV.8. Conclusions.....19

V Coherent interactions in mercury vapor

V.1. Introduction

V.2. Theory.....20

V.3. Source developments.....22

VI Use of multiple pulse sequences.....23

VII References.....24

VIII Personnel.....26

IX List of Publications under grant AFOSR-82-0332.....27

APPENDIX A: Spatial and temporal properties of a tunable picosecond dye laser oscillator-amplifier system.

APPENDIX B: Theory of coherent interactions in mercury.

APPENDIX C: Design of a 50 fxec linear laser.

APPENDIX D: Multiphoton ionization under sequential excitation by coherent pulses.

Grant AFOSR-82-0332, Final Technical Report
(October 1982-December 1984)

STUDY OF VACUUM ULTRAVIOLET GENERATION BY COHERENT RESONANT FREQUENCY MIXING IN METAL VAPORS

I. GENERAL OBJECTIVES

The general long term goal of this project is to demonstrate an efficient method of frequency up-conversion, using simultaneously "resonant" and "coherent" enhancement. Conditions of multiphoton resonances are sought to enhance the nonlinear susceptibility responsible for harmonic generation. Coherent propagation effects are exploited to minimize depletion of the fundamental by the (multiphoton) resonant absorption and by photoionization, and to maximize the distance over which phase matching is maintained. We have demonstrated experimentally the theoretical maximum conversion efficiency of 0.5%, for the full beam cross section, in lithium vapor (section IV). A theoretical study has been made in preparation for experiments of 5^{th} harmonic generation in condition of four photon resonant coherent interaction in mercury vapor (section V).

This project leads also to a analytic technique to measure nonlinear susceptibilities. The measurements of third harmonic versus phase difference between a pair of exciting pulses presented in section IV enabled us to measure for the first time the phase angle of the nonlinear susceptibility.

Harmonic generation is only one of many applications that can be enhanced by multiphoton resonant coherent interactions. It is shown in section VI that a technique of multiple pulse sequences can be used to achieve spectral selectivity with ultrashort pulses, even in broadband molecular systems.

II. BASIC APPROACH

With the availability of shorter and shorter pulses, hence higher peak intensities, one might expect simultaneous improvements in nonlinear optical techniques such as sum and difference frequency generation. However, as the pulse become shorter, their increased bandwidth will interact with a larger number of levels of the atom, leading to very complex propagation characteristics, and increasing losses of energy through multiphoton absorption. As the pulses become shorter than the phase relaxation times of the media involved, there is a possibility to reverse the energy transfers between matter and radiation, and return to the fields the energy once lost by absorption. The purpose of this study is to find a way to take advantage of the reversibility of light matter interaction with ultrashort coherent interaction, to enhance the efficiency of sum frequency generation. The general method sought is to "prepare" the medium with a first pulse, and use a second pulse to convert back to the radiation field, at the desired wavelength, all the energy lost to the medium by the first pulse. In this particular project, the nonlinear medium is excited by a sequence of two pulses.

One may already wonder at this point whether it makes sense to divide the available power into small fragments. Is the total excitation not just the sum of that by each of the successive pulses? Not if the pulses are shorter than the phase memory of the matter - collision time or internal phase relaxation time -. The relative phase of the pulses determine which way the energy is to flow - that is whether there will be absorption or stimulated emission.

There is a quantum jump in complexity in going from one to two pulse excitation - because one is adding a dimension to the problem: **the phase.** The experimental requirements are rather stringent: the source has to be able to generate high power tunable pulses with a uniform wavefront - an essential condition in order to be able to define the phase - . One needs to be able to adjust the relative phase and delay between the two pulses of the sequence. The phase or frequency modulation of the pulses should be small, or it would not be possible to define an average phase for each pulse. Finally, resonant coherent interaction is strongly dependent upon the pulse shape and frequency, which are not particularly easy to determine with picosecond pulses.

III. OVERVIEW OF THE SYSTEMS UNDER INVESTIGATION

The relevant energy levels of the two atomic system that have been the object of this investigation are sketched in Fig. 1 below.

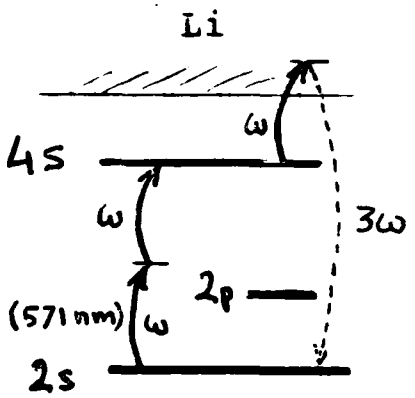

Figure 1a
Relevant energy levels of lithium.

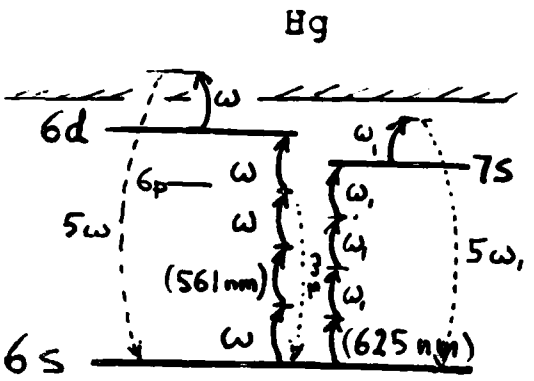

Figure 1b
Relevant energy levels of mercury.

The first and simplest resonant enhancement to be considered for harmonic generation is the two-photon resonance. As an example, we have chosen to conduct experiments on the 2s - 4s transition in lithium vapor (figure 1a), for which all the relevant parameters have been calculated [1]. This atomic system is (two-photon) resonant for radiation at 571 nm. The proper partial vapor of magnesium will phase match the third harmonic and fundamental. The energy density required to significantly populate the 4s state is of the order of 50 mJ/cm^2. Some of the experimental difficulties to overcome are:

a) Generation of pulses of 6 psec duration, 1 mJ energy, with a flat wavefront, a Gaussian beam profile, and no temporal phase modulation.
d) Splitting of these pulses into a sequence of two identical pulses of well defined relative delay and phase.
e) Monitoring the phase difference between the two pulses of the sequence.
b) Preventing temporal and spatial phase distortion in the amplifier and in the heat pipe.

c) Production of an homogeneous mixture of Li and Mg near 1,000 ^{o}C.
d) Finding a "transient phase matching condition" that is entirely different from the phase matching condition at moderate intensities (or in the absence of coherent interactions).

A two-photon resonance in a four photon process - as the one involved in third harmonic generation - is a very particular case of resonant interaction. Indeed, as shown in reference [1], the pulse energy is the main parameter determining the relative population transfers. For pulses shorter than the phase relaxation (elastic collision time), the time is only a scaling parameter (for instance, shorter pulses will produce the same amount of third harmonic than longer pulses of the same energy). This is non longer the case when higher order resonances are involved.

The next system under investigation is mercury vapor excited in conditions of four photon resonance (figure 1b). There are two resonances that are accessible to amplified picosecond dye lasers: the 6s - 6d transition (four photon resonance for radiation at 561 nm), and the 6s - 7s transition (four photon resonance for radiation at 625 nm). The case of a four-photon resonance is much more complex than that of a two-photon resonance, because Stark shifts of various order become important at the intensities required for effective four-photon excitation. In addition, the pulse duration becomes an important parameter, since, at constant pulse energy, the population transfers will be largest for the shortest pulses.

In the particular case of the 6s - 6d transition of mercury, the 6p level is close to 3/4 the energy of the 6d level, resulting in a resonant enhancement of the Stark shift of the 6s - 6d transition. This Stark shift is so important that, for femtosecond pulses of 5 J/cm^2 tuned to 1/4 of the 6s - 7s transition frequency, the 6s - 6d transition becomes also near resonant!

IV. COHERENT INTERACTIONS IN LITHIUM VAPOR

IV.1. The Laser Oscillator-Amplifier System

We have constructed a laser oscillator-amplifier system [2] capable of producing single pulses of 1 mJ energy, at a repetition rate of 10 Hz, tunable around 570 nm. The amplifier is sketched in Fig. 2 below. Design details can be found in Appendix A (ref. 2). The first two stages are pumped transversally, and the last one longitudinally. Coupling between the first stages is minimized by synchronizing the first stage at the leading edge, while the second stage is synchronized at the trailing edge of the pump pulse. The amplified spontaneous emission (ASE) after the last stage is approximately 1% of the pulse energy, without the use of any other isolator than a direct vision prism between the two first stages. Several dyes and solvents have been investigated, which have a maximum gain and a minimum absorption at 570 nm. The purpose of the small absorption for the unpumped dye is to have the amplifier transparent to the unamplified beam,

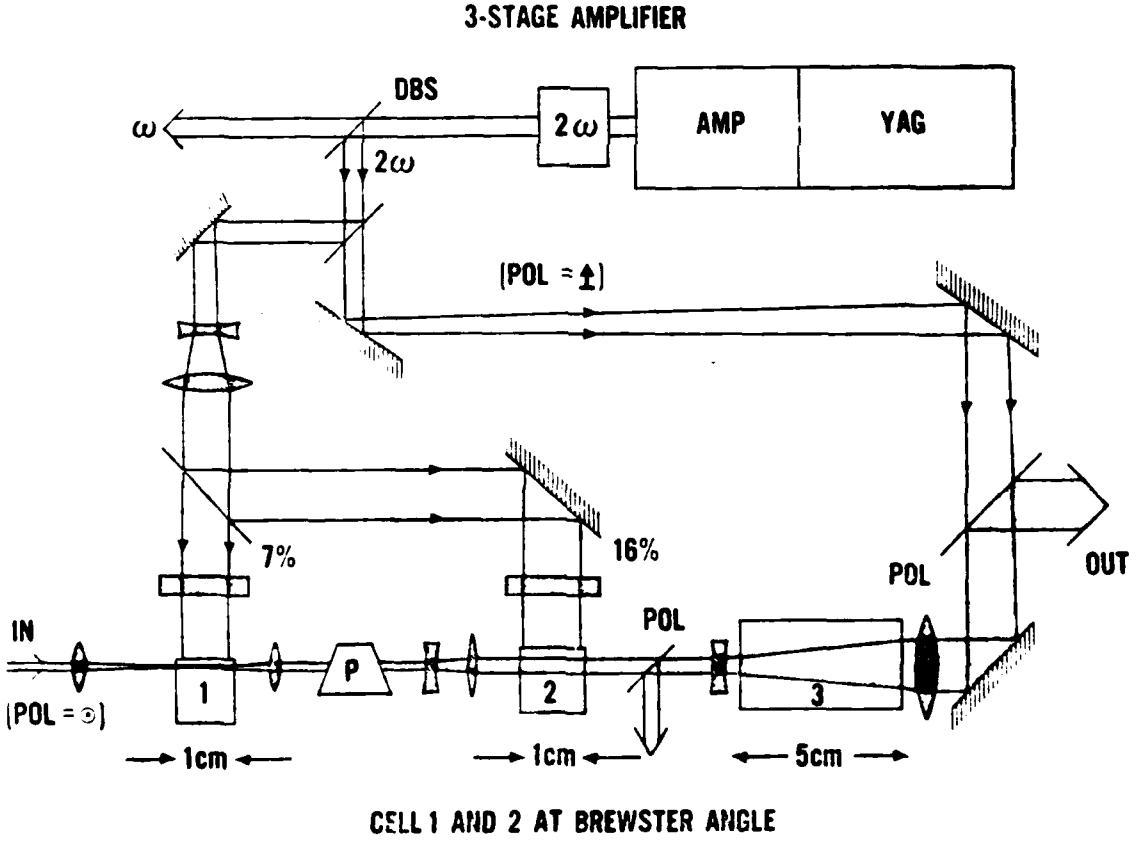

Figure 2 Sketch of the Laser Amplifier.

an essential condition to perform the critical alignments of the interferometers used for the analysis of time and space coherence. The combination of Hexafluoroisopropanol (HFI) with Rhodamine 6G shifts sufficiently the absorption and fluorescence spectra of Rhodamine 6G to meet the conditions of no absorption and maximum fluorescence at 570 nm. In view of the high costs of HFI mixtures of water and HFI were investigated, which were reported to combine the spectral shift of HFI and the thermal conductivity properties of water [3]. Unfortunately, the desired spectral shift were not found in the water solutions, which separated into two unmiscible components after a few days. For operation at 570 nm, the latest choice of dye solutions is:

1st stage: Rhodamine 6G .18 mM/l in Ethanol.
2nd stage: Rhodamine 6G .14 mM/l in Ethanol.
3rd stage: Rhodamine 6G in Water and Ammonix 0.01 mM/l.

Beam Profile

Careful position of the pump beams relative to the amplified beam in the last two stages provides complete control over the spatial intensity distribution, from "square" (fig. 3a) to Gaussian (fig. 3b).

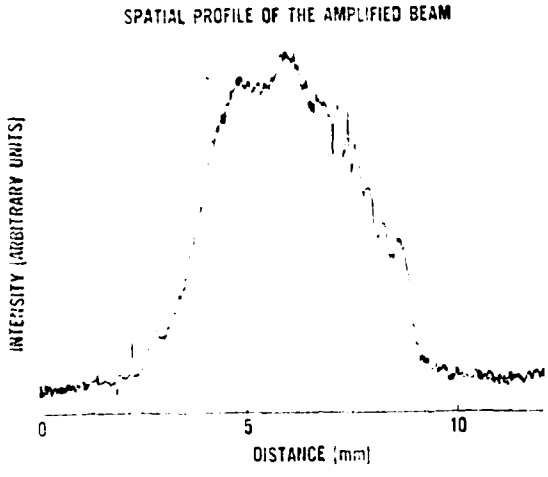

Figure 3a

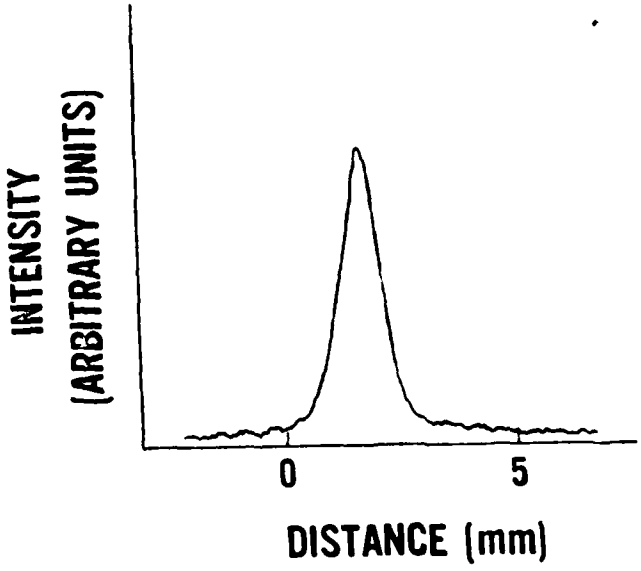

Beam Profile

Figure 3b

Spatial Coherence of the amplified pulse is demonstrated by achieving uniform extinction of the beam in a Mack Zehnder interferometer.

Temporal Coherence The measurement of temporal coherence is crucial to the experiments of coherent propagation, and has been used to test the laser sources, the scanning technique, and the data acquisition system. Measurements as the one shown in Fig. 4 indicate that the amplifier does not introduce any phase modulation. The amplified pulse can best be represented by a Gaussian temporal profile with a phase modulation $\varphi(t)$ proportional to the pulse intensity ($\varphi = 1.43\ E^2$). This is the first time that the technique of interferometric autocorrelations [5] has been applied to the chirp determination of synchronously mode-locked lasers. The small phase modulation that we measure corresponds to an increase of bandwidth duration product of only 10 %, hence is too small to be determined by conventional spectral measurements.

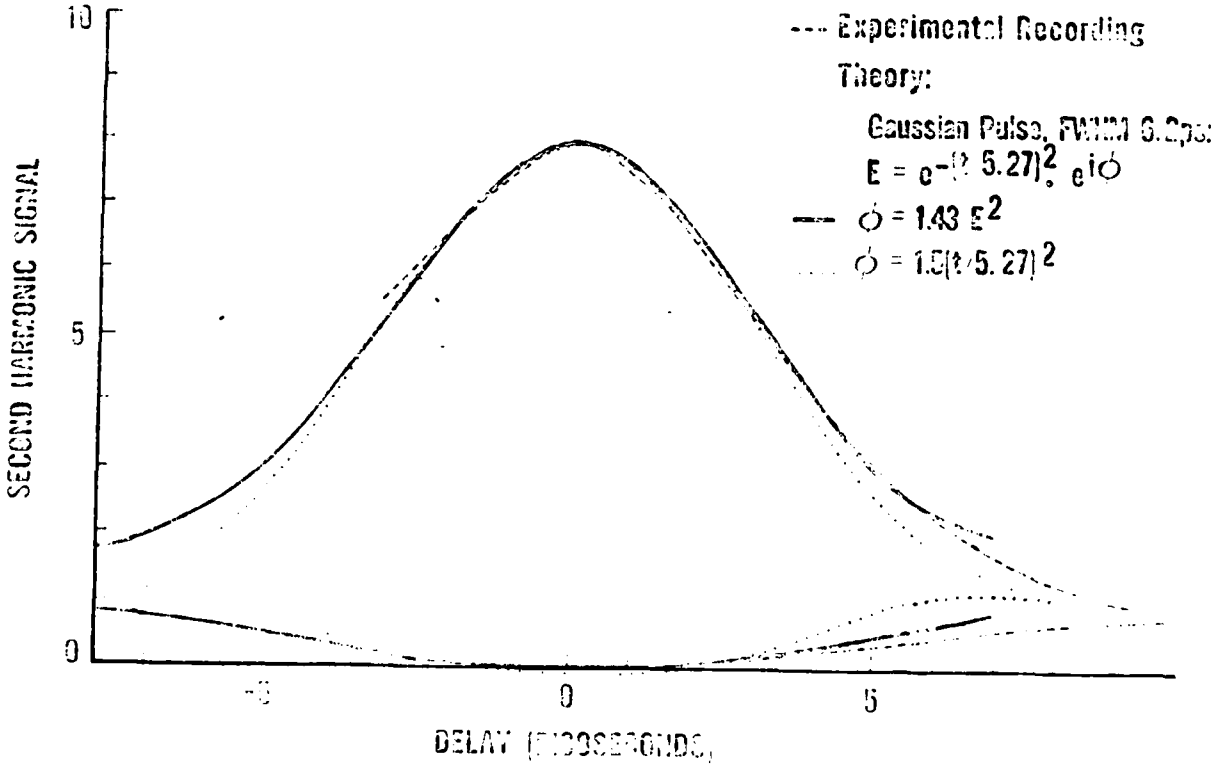

Figure 4
Interferometric autocorrelation of the 6.2 psec pulses

IV.2. The Lithium-Magnesium Heat Pipe

Three successive prototypes had to be constructed to evolve from the basic heat pipe design of Vidal and Cooper [5] to an instrument which confines a homogeneous, uniform and transparent mixture of lithium and magnesium vapors, and that can be operated continuously for several days at 1000 ^{o}C. The rather slow data acquisition process (limited essentially by the slow repetition rate of the laser oscillator-amplifier chain) imposes severe constraint not only on the source stability, but also on all other components of the experiment. Obviously the heat pipe has to be perfectly sealed, but in addition the outgassing of the walls has to be continuously and selectively (i.e. without pumping the He buffer gas) eliminated during the experiment. The selective pumping was achieved with cryogenically cooled molecular sieves. Another problem is a condensation of solid lithium at the edges of the hot zone. The resulting accumulation over several hours of an annular ridge of solid has been sufficient to obturate the optical path, in the first two prototypes. The problem of accumulation of lithium near the ends is alleviated with the larger final version of the heat pipe, but it still limits its continuous operation to roughly one week.

Phase matched third harmonic generation measurements have been made in homogeneous mixtures of lithium and magnesium. The relatively low vapor pressure of solid magnesium causes it to escape (by sublimation) from the central region of the heat pipe during the heating period. Once the lithium has melted, the magnesium is trapped with the lithium vapor in the central region. Attempts to introduce the magnesium in the hot heat pipe (after the lithium has melted) have been abandoned as too hazardous.

A fourth heat pipe which consists in an upper and lower plan circular electrode with a central mesh, separated by a pyrex cylinder, has been constructed. This heat pipe is intended for measurement of photoionization.

IV.3. The Data Acquisition System

The experimental set up is sketched in figure 5. The beam from the oscillator-amplifier is sent through a "pulse sequencer, which splits each pulse into two pulses of continuously increasing relative phase and delay. The two pulse sequence energy is monitored by D_3 before being sent through the heat pipe. The transmitted signal(s) is (are) monitored by D_4. All detectors at the fundamental laser wavelength (D_1, D_3, and D_4 are combination of frequency doubling KDP crystals, filters, and UV detectors. In addition to discriminating the amplified pulses from the nonamplified pulse train (which has a higher average power), this second harmonic detection scheme provides more accurate transmission measurements.

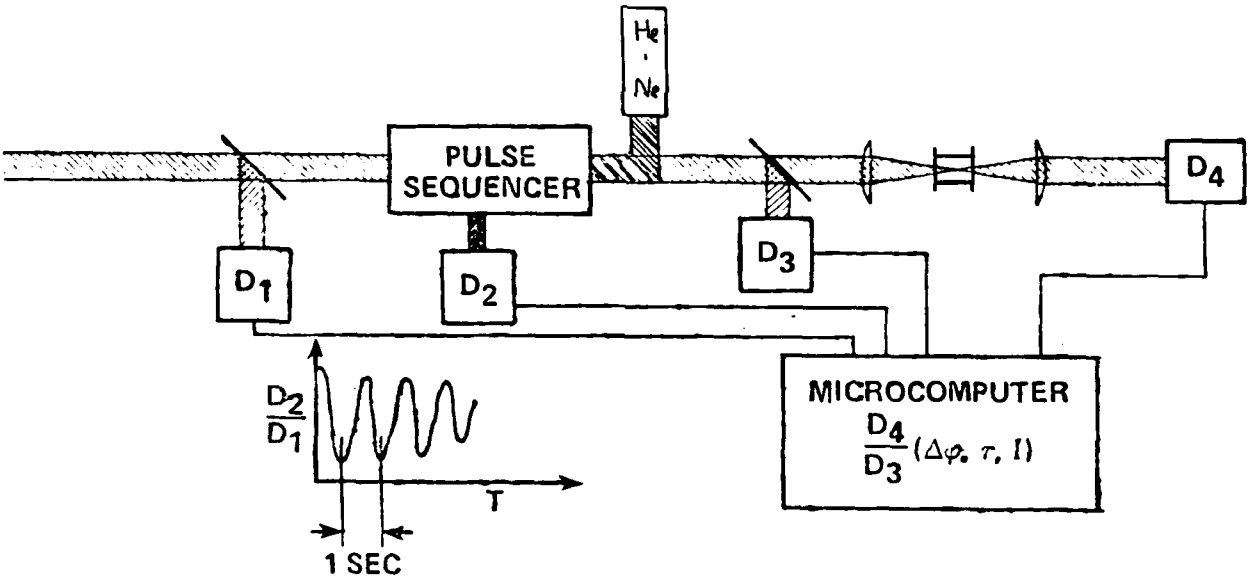

Figure 5: Experimental set up

A Mack Zehnder interferometer[7] is used to create the sequence of two pulses with continuously increasing phase and delay (as needed for the experiments of coherent propagation, as well as for the analysis of pulse coherence). The (collimated) beam produced by the amplifier is split into two parts by an adjustable beam splitter (based on frustrated total internal reflection). One beam is given a fixed delay by a combination of fixed prisms optically contacted together, while the other beam is sent through an adjustable optical delay line, before being recombined with the first one with another adjustable beam splitter.

The phase and delay are really one single parameter. As the delay is scanned continuously, the phase increments by 2π for every delay increment of a wavelength of .57 micron. With a pulse repetition rate of 10 pps, the translation speed of the delay arm of the interferometer should be less than .1 microns/s in order to have at least 20 data points per period! Such a low speed is incompatible with a smooth continuous motion. Because of solid friction in the drive, the delay stops moving, then jumps a wavelength or more, making it impossible to maintain and determine the delay and phase with interferometric accuracy. The solution is to maintain the translation speed high enough for continuous motion, to monitor continuously the phase, and to store the data points of successive periods (for example 100 periods) into an "equivalent" period. The exact value of the phase is determined by monitoring the transmission of a He-Ne laser through the same delay line. This monitoring is essential, because even the best synchronous motor drive for the delay line does not provide a continuous speed for the translation stage, because of the errors introduced by reduction gears. The exact optical delay X in the pulse sequencer is determined (with an accuracy better than 0.03 micron) from the $(\cos\ )^{-1}$ of the He-Ne laser intensity recorded by the detector D_2.

The amount of averaging that can be done is directly related to the duration and coherence of the pulses. The criteria are those of the slowly varying approximation: the averaging can only be performed over the number of cycles over which the pulse **amplitude** and **phase** can be considered to be constant. With our 6.2 psec pulses, the maximum number of periods over which the data could be averaged is at most N = 300. As the delay is being continuously scanned, the data are accumulated for a total delay

increment of $X_{max} = N\lambda$ (where λ is the wavelength of the pulses), and sorted according to their relative phase:

$$\Delta\varphi = 2\pi (X - n\lambda)/\lambda$$

The accuracy of the averaging process is directly related to the accuracy in the determination of the wavelength. If, for instance, we choose to divide the 2π phase interval in 25 segments, and average the data over N =100 periods, the maximum allowable error in the wavelength determination is $\lambda/2500$. Fig. 6 below shows an example of such an averaging over 100 periods, of the second harmonic of the signal created by the pulse sequencer, as recorded by D_3, normalized to the second harmonic of the pulse from the laser source, as recorded by D_1. In that particular recording, the data points were sorted in 25 phase sectors.

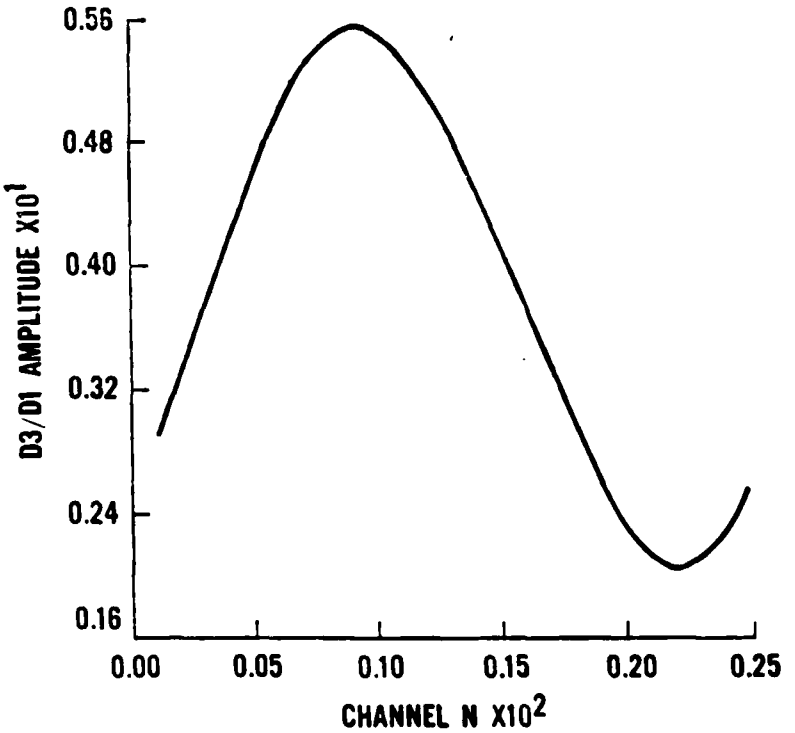

Figure 6 Recording of signal versus phase (averaging over 100 periods, 25 phase sectors)

The accuracy of the averaging process can be improved by computing, for each phase sector, the average phase as well as the average signal. This procedure is particularly useful in the cases when the signal has a complex dependence on the phase difference, as in the examples shown below.

Finally, since the interaction is energy dependent and the gain factor of the amplifier fluctuates, the data are grouped according to the input energy as recorded by the detector D_1.

IV.4. Nonlinear Transmission

With the heat pipe cold, the detectors in D_3 and D_2 record the interferometric autocorrelation shown in Fig. 4. The data acquisition microcomputer stores also the average of this function over each period, which is the intensity autocorrelation shown in Fig. 7a. Depending on the tuning of the laser and its peak power, a variety of deformation of the transmitted autocorrelations is observed. For instance, in the recording of Fig. 7b, taken for a pressure of 10 torr of lithium vapor, it appears as if the top half of the intensity autocorrelation has been "chopped off". A similar change is observed for the interferometric autocorrelation.

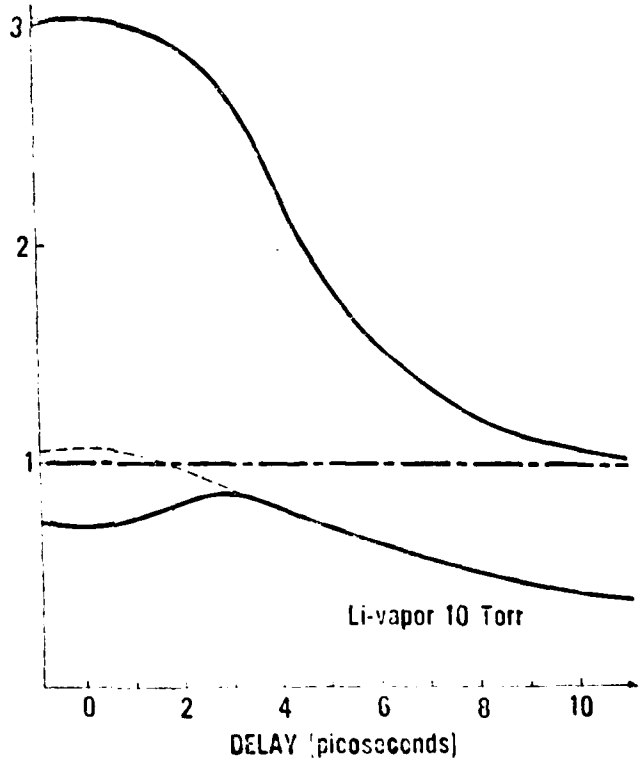

Figure 7 Fringe averaged recording on D_3 (a) without lithium (top figure) and (b) with 10 torr of lithium (lower figure).

The tuning characteristics of the nonlinear transmission are illustrated by the computer simulations of Fig. 8, which show successive interferometric (top) and fringe averaged (bottom) recordings of the second harmonic of the transmitted signal versus delay, for various detunings. The pulse "area" (the time integral of the generalized Rabi frequency, which is proportional to the pulse energy density) is equal to 1. The calculations are carried out in the "thin sample" approximation (negligible propagation effects). Far below resonance (right side of Fig. 8, $\Delta\omega = 12\ 10^{11}\ s^{-1}$, the pulse doesn't interact with the line, and the autocorrelations are unchanged from the ones without lithium. At a detuning of $9\ 10^{11}\ s^{-1}$, which corresponds to 6 inverse pulse-widths below resonance, the top of the autocorrelation is truncated. This is because near zero delay, the Stark shift corresponding to the coherent superposition of the two pulses is sufficiently large to bring the resulting peak electric field into resonance. This corresponds also to the situation shown in the experimental recording of Fig. 7.

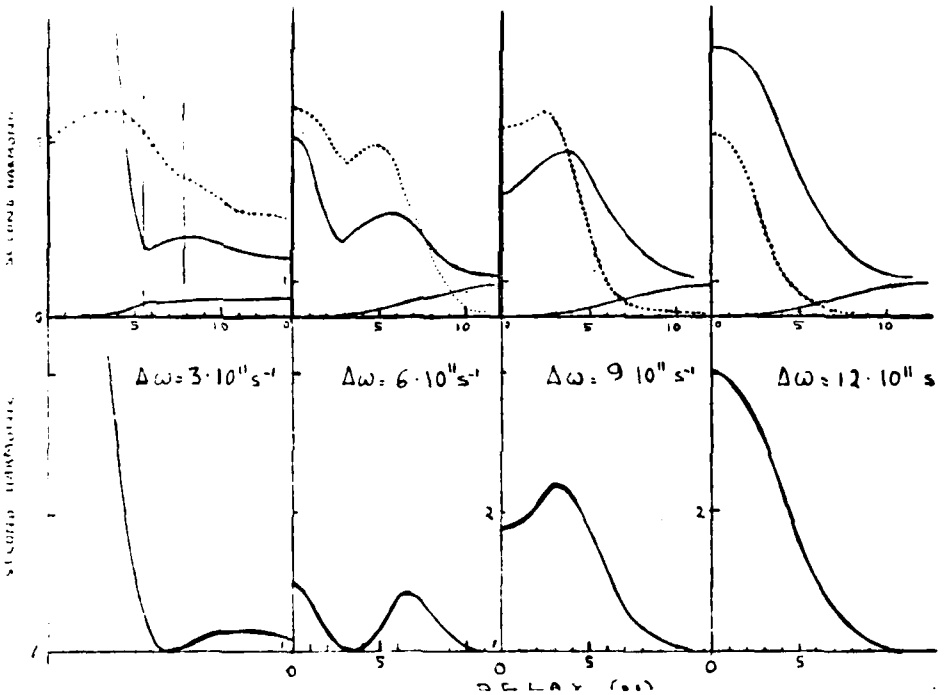

Figure 8: Successive Interferometric (top) and Fringe Averaged traces of the second harmonic of the transmitted signal versus delay, for various detunings (calculated).

With increasing laser frequency (decreasing detuning), the "hole" burnt by the resonance line in the autocorrelations moves to larger delays. In the last case, the coherence region extends very far in the wings of the interferometric autocorrelation, far beyond the limits of pulse overlap. Near zero delay, the second harmonic of the transmitted signal can be larger than that of the incident pulses, because of pulse reshaping (shortening).

The third harmonic intensity varies also with delay, frequency and phase, The maxima (for each 2π phase interval) of the third harmonic varies with delay as shown by the dashed curves in Fig. 8. The envelope of the third harmonic versus delay far below resonance ($\Delta\omega$ = 12 10^{11} s^{-1}) is a third order interferometric autocorrelation, with a peak to background of 32 to 1. In general, the shape of the upper envelope of the third harmonic versus delay follows qualitatively that of the second harmonic signal versus delay, with the largest harmonic conversion being generally close to zero delay. The situation is different in the case of propagation through thick samples. For an interpulse delay between 5.5 and 8 psec, at 3 10^{11} s^{-1} below resonance (region indicated by vertical lines in Fig. 8), the anomalous transmission of the "90° phase shifted" pulse sequence exceeds by one order of magnitude the "in phase" sequence, because of a near lossless propagation of the second pulse [1]. Phased matched third harmonic generation should reach peak efficiencies (total energy conversion efficiency over the entire beam cross section) of the order of 1% in these conditions.

IV.5. Data on Nonlinear Transmission and Harmonic Generation

The data of nonlinear transmission and harmonic generation versus delay, taken for various detuning conditions, show the characteristic patterns of Fig. 8. As in the theoretical simulations, as the detuning (laser below resonance) is increased, the "dip" in the upper envelope of the interferogram of the transmitted signal (in second harmonic) moves towards the center of the autocorrelation (for that detuning, only the sum of the two pulses at zero delay has a sufficient Stark shift to "reach" the resonance). A typical recording is shown in Fig. 9. The dashed line (triangles) is a recording of the interferometric autocorrelation of the pulses. The dotted (squares) and solid (circles) lines in Fig. 9 are the envelope of the recording of the transmitted signal (in second harmonic) and of the third

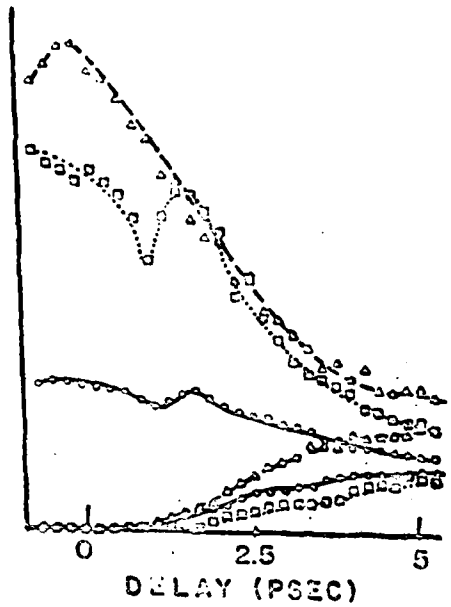

Figure 9
Envelope of the incident (dashed lines)
and transmitted signal (dotted lines)
and of the third harmonic (solid lines).

harmonic, respectively. The "dip" at a delay of 1 psec corresponds to the delay at which the Stark shift due to the coherent superposition of the fields equals the detuning. Another recording taken closer to resonance is shown in Fig. 10.

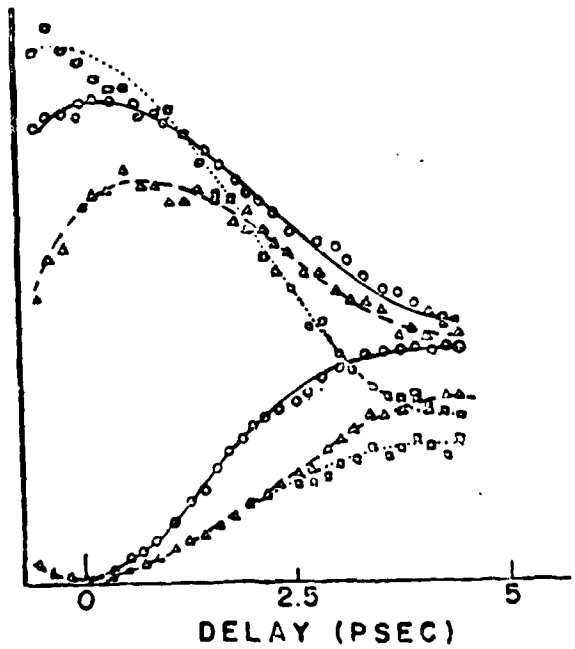

Figure 10

Consistently with the numerical calculations, the transmitted signal near zero delay appears to be **larger** than the incident signal. This apparent amplification is merily the manifestation of pulse reshaping (compression) near zero delay. The second harmonic of the (shorter) transmitted intense pulses near zero delay is larger than the second harmonic energy contained in the incident pulses.

IV.6. Phase Dependence.

Figure 11 shows, for a particular inter-pulse delay of 2 psec, the fundamental (measured in second harmonic) before (dashed line) and after (dotted line) the lithium heat pipe, as well as the third harmonic (solid line) as a function of the relative phase between two pulses. The phase interval has been divided in 16 sectors. The recordings of Fig. 11 represent the average of 100 successive periods. The data points at a delay of 2 psec in Fig. 9 represent the maxima and minima of the curves of Fig. 11. For this relatively small delay (compared to the pulse duration), the phase dependence is dominated by the constructive-destructive interferences of the overlapping pulses at the fundamental wavelength. For large delays, the second pulse is interfering constructively and destructively with the multiphoton excitation created by the first one, in addition to interfering partially with itself (in the wings of the pulse). At phase shifts of 90° and 270 °, the second pulse is amplified by two-photon stimulated emission, resulting in an enhanced transmission. For delays exceeding the pulse duration, the transmitted signal versus phase has a periodicity of π.

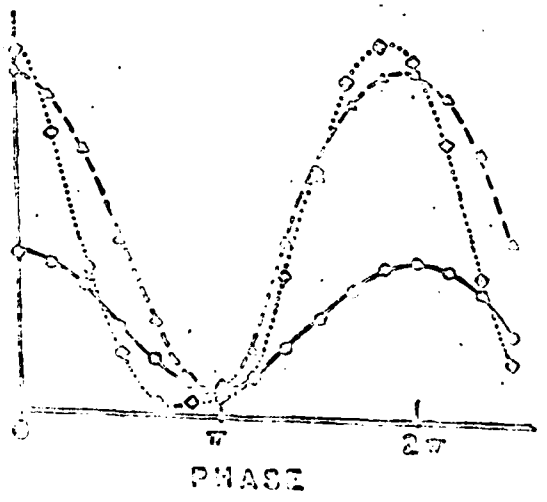

Figure 11

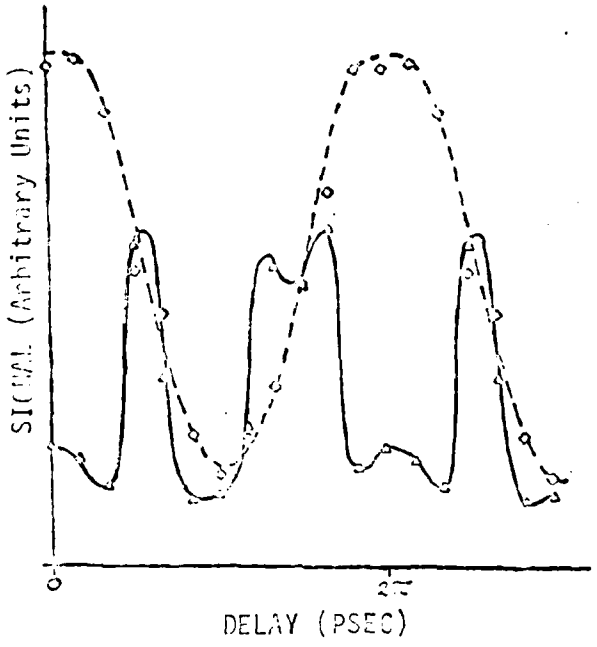

Figure 12: Transmitted signal and third harmonic versus phase for a delay of 2.5 psec.

At intermediate delays such as in the case of Fig. 12, the transmitted signal (dashed line) is still dominated by the constructive-destructive interferences in the region of pulse overlap. However, the third harmonic shows the predicted enhancement at dephasings of 90° and 270 °. There is another interesting feature in Fig. 12, that also appears in all measurements corresponding to large interpulse delays. The periodic third harmonic signal is dephased with respect to the transmitted signal. This dephasing angle is $-\pi/6$, and corresponds to the phase angle of the complex third order susceptibility. We have found indeed in previous theoretical work [1] the third harmonic generation per unit "characteristic distance" [8] to be proportional to the quantity:

$$\zeta_{21} = \sum \left[\frac{\mu_{2\ell} \mu_{\ell 1}}{\omega_{\ell 1} - 5\omega} + \frac{\mu_{2\ell} \mu_{\ell 1}}{\omega_{\ell 2} + 5\omega} \right]$$

The imaginary part of this nonlinear coefficient - hence the phase angle of $-0.481 \simeq -\pi/6$ - is due to the contribution of the continuum. The measurement of the phase dependence of the third harmonic offers thus a unique way to measure the contribution (to the third order susceptibility) of the continuum relative to that of the resonance , or more generally, the phase angle of the nonlinear susceptibility.

IV.7. **Phase Matching**.

Theoretical calculations [1] predicted a ratio of 2 to 1 for a phase matched lithium-magnesium mixture in conditions of coherent propagation (a ratio completely different from that corresponding to "incoherent" or "small signal" phase matching). The transmitted signal versus delay and the envelope of the third harmonic versus delay in a 2/1 mixture of magnesium/lithium are shown in Fig. 13. A maximum conversion efficiency of 6% was predicted for an infinite plane wave, propagating through at least four two-photon characteristic distances (one characteristic distance is 1.4 cm at the operating pressure of 10 torr). The maximum achievable conversion efficiency over the entire cross-section of a finite beam is of course smaller by approximately one order of magnitude. A conversion efficiency between 0.5 and 1% is measured. Even though these numbers appear very

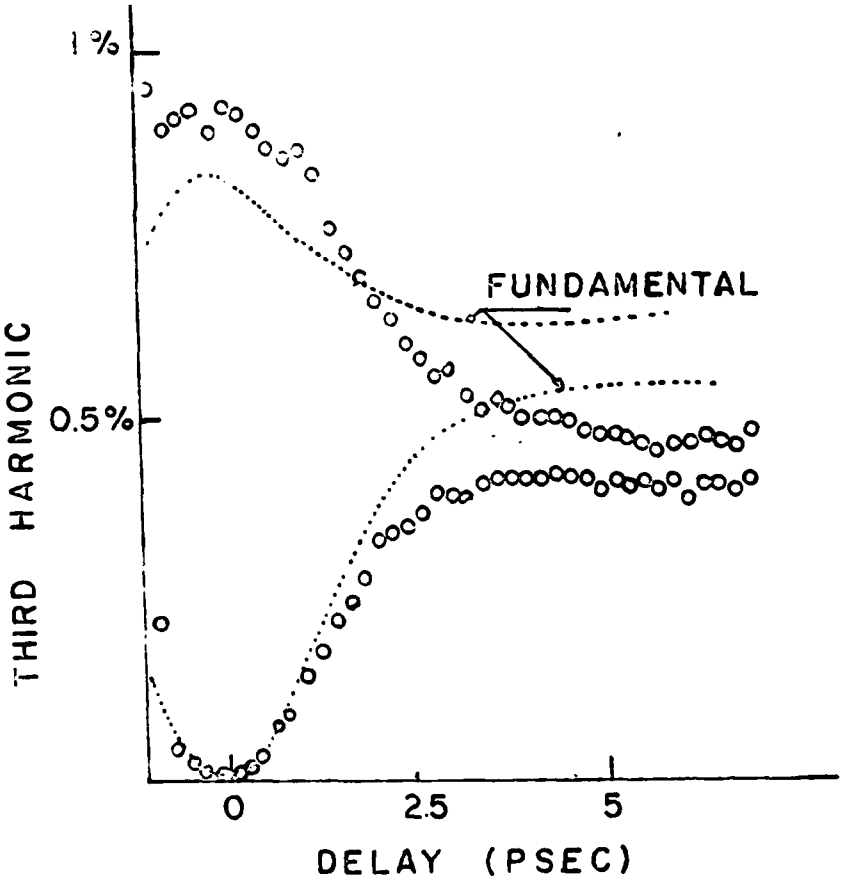

Figure 13
Third Harmonic and transmitted signals versus delay.

close to the theoretical limit, it should be noted that the measured efficiency is still limited by the power available from the source. Indeed, the confocal parameter of the beam focused in the heat pipe is only 10 cm, hence too short for the requirement of uniform beam cross section over that distance. The energy density in vacuum varied in this distance from 50 mJ/cm^2 to 100 mJ/cm^2 (while the thick sample calculation call for a constant energy density of 100 mJ/cm^2 over that distance). The similarity between fig. 13 and the "thin sample" simulations of Fig. 8 is due to the too short confocal parameter of the focusing in the sample. An additional amplification stage would be required to reach conversions over 1%, peaking at delays larger than 2 psec.

IV.8. **Conclusions**

Enhancement of third harmonic generation through coherent interactions in conditions of two photon resonances has been demonstrated for the first time experimentally. The agreement between theoretical prediction and the experimental results indicates that self focusing and defocusing effects are not important enough to affect the conversion efficiency.

This series of experiments demonstrates that it is possible to construct a picosecond dye amplifier with a gain over 10^6 without introducing spatial (wavefront) or temporal (chirp) phase distortion. Phase distortion due to convection currents in the 1000^oC heat pipe were also found to be negligible.

Recording of the third harmonic and transmitted signal versus phase enabled us to measure, for the first time, the phase angle of the third order susceptibility responsible for third harmonic generation. The corresponding imaginary part of the nonlinear susceptibility was seen to match exactly the calculated contribution of the continuum.

The purpose of the experiment in lithium was to demonstrate the points cited above, which can be transposed to any scheme of up-conversion in presence of a two-photon resonance. The case of a higher order (four photon) resonance is considered in the next section.

V COHERENT INTERACTIONS IN MERCURY VAPOR

V.1. Introduction

From the theoretical point of view, the case of a two photon resonance is a very particular case of interaction where all terms are second order in the field. For a negligible Stark shift and photoionization, there is only one parameter (apart from a scaling factor) distinguishing one atom from another: the ratio of the probability of third harmonic generation to that of two-photon stimulated emission (ζ_{12}/γ_{12} in the notations of ref. 1). There is no optimal pulse duration, within the constraint that the pulse duration be shorter than the elastic collision time.

The case of higher order resonances (N) is much more complex: the equations will contain terms of all order up to the N^{th}. The case of four photon resonant excitation of the 6s - 7s transition of mercury vapor is particularly interesting but complex, because of a near three photon resonant enhancement through the 6p level. A theoretical investigation of coherent propagation and harmonic generation in mercury vapor has been completed, using the same formalism as for the study of harmonic generation in lithium vapor [1]. Preparations for an experiment to complement the theory have been made (laser source, vapor cell).

V.2. Theory

As in the case of a two photon resonance, a generalized Rabi frequency can be defined, which is here proportional to the fourth power of the electric field of the light at the fundamental frequency. However, the analogy stops here, because the presence of terms of lower order makes it impossible to express all electric field related quantities in units of the Rabi frequency.

The equations describing coherent four-photon resonant propagation and third and fifth harmonic generation in mercury vapor are detailed in Appendix B. The dipole matrix elements needed to evaluate all the coefficients of these equations were calculated from the absorption coefficients corresponding to the main transitions. Some major conclusions from the theory are listed below.

- For large delays, the phase dependence of the transmitted signal, the third and fifth harmonic have a periodicity of $\pi/2$.
- For picosecond pulses at 560 nm, an energy density of the order of 1 J/cm^2 is required to significantly populate the upper level of the resonant transition.
- For femtosecond pulses at 620 nm, the energy density required to pump significantly the 7s level is of the order of 100 mJ/cm^2.
- The proximity of the 6p level at 3/4 of the 6s - 6d transition results in an anomalously large Stark shift and an enhancement of third harmonic generation.
- A large photoionization cross-section from the 6d level would prevent efficient conversion to higher harmonics in a two pulse sequence.

The theory leaves several basic questions unanswered, that will have to be resolved by experiments. First, the Stark shift of the 6s - 6d transition (4 photons at 560 nm) is so large, that high energy femtosecond pulses at 620 nm could be simultaneously resonant with the 6s 7s and with the 6s 6d transitions! While it is likely that the theoretical model chosen breaks down in that situation, there might still be a large enhancement of the non-linear susceptibilities.

Another basic unanswered question pertains to the large photo-ionization from the excited level. Has the photoelectron lost complete memory of its position in the Hg atom, even 10 fsec after its ejection? This question can be tested by counting the number of ions created by a pair of closely spaced pulses, as a function of their relative phase.

V.3. Source Developments

For a given pulse energy, the shorter pulses of higher peak intensity will be the most efficient in exciting a multiphoton resonance of order higher than 2. We have therefore started the development of a femtosecond laser oscillator to replace the 6 psec synchronously mode-locked laser. That laser oscillator combines the features of the passively mode-locked dye laser [9] with the tunability of the synchronously mode-locked laser. Passive mode-locking is achieved in an "antiresonant ring" located at one end of the cavity [10]. The antiresonant ring is mounted on a translation stage, which allows continuous tuning of the cavity length, an essential feature for synchronous mode-locking [11]. In recent tests, passive mode-locking alone has provided highly stable operation with 50 fsec pulses, and an average output power of 50 mW [12]. Geometrical astigmatism compensation is used to maximize the intracavity power density in the saturable absorber [12] (Appendix C). The pulse shape and phase modulation are accurately characterized, using techniques of pulse shape and chirp determination that we recently developed [5]. The "downchirp" of the pulses can be adjusted to yield pulse compression instead of pulse broadening through the normally dispersive amplifier chain. A hybrid passively-actively mode-locked laser based on this design is presently being tested. It is hoped that the hybrid laser will provide a higher output power (100 mW) and easier tunability than the purely passively mode-locked laser. It should be noted however that the present tunability range of the purely passively mode-locked antiresonant dye laser (605 to 630 nm) is quite adequate to study coherent four photon resonant interaction on the 6s - 7s and on the (Stark shifted) 6s - 6d transitions of mercury. The accurate knowledge of the pulse shape and modulation[5] is a particularly important asset in the study of coherent effects in photoionization.

The use of shorter pulses makes it possible to use much higher pressures in the sample cell (since the requirement that the collision rate be slower than the inverse pulsewidth is relaxed by two orders of magnitude). The possibility of using higher pressures, smaller confocal parameters, alleviates much of the difficulties associated with the design of a sample cell. A short mercury heat pipe has been constructed, in which two stainless steel cones serve the dual purpose of ion counting electrodes and return channel for the condensing mercury.

VI USE OF MULTIPLE PULSE SEQUENCES

We have extended the theory to the use of multiple pulse sequences in the study of multiphoton ionization of lithium. The results of this work are contained in a paper published in Phys Rev. [13] and included as Appendix D. This theoretical study shows how random pulse sequences should be used to study the influence of source coherence on a multiphoton process. Another basic point arising from this theory is that regular pulse sequences can provide spectral selectivity well beyond the pulse bandwidth. For instance, by tuning the average frequency of a train of 10 pulses, the number of ions produced in lithium vapor (condition of two-photon resonance) versus laser frequency displays a series of peaks reminiscent of the Fourier spectrum of the excitation. The width of these individual pulses can be used as a measure of the photoionization rate from the excited (4s) level.

The basic conclusion from this theory is that the use of pulse sequences offers a solution to the conflicting requirements of spectral selectivity and high peak intensities needed to study multiphoton processes. This conclusion applies to molecules as well as to atoms. The study has been recently extended to multiphoton vibrational spectroscopy. Pulse sequences have been designed to excite to a high energy level an anharmonic ladder of levels. The relative phase between successive pulses determines the direction of flow of energy within the molecule: whether there will be absorption of emission of a photon within the ladder of levels. Calculations of multiphoton excitation of an anharmonic ladder of vibrational-rotational levels have been made. The model chosen was that of the molecule CH_3F. The calculations show [14, 15] that simple four or five pulse sequences can be designed to bring most of the population in the level $v = 5$. These particular pulse sequences result in a cooling of the rotational temperature in the excited state. Pulse sequences offer thus the possibility of achieving vibrationally as well as rotationally selective multiphoton vibrational excitation of molecules.

REFERENCES

1. J.-C. Diels and A. T. Georges, "Coherent Two-Photon Resonant Third and Fifth Harmonic VUV Generation in Metal Vapors", Physical Review A19, 1589 (1979).

2. H. Vanherzeele, H. J. Mackey, and J.-C. Diels, "Spatial and Temporal Properties of a Tunable Picosecond Dye Laser Oscillator-Amplifier System", Applied Optics **23**, 2056-2061 (1984).

3. F. P. Schäfer, private communication.

4. H. Vanherzeele and J.-C. Diels, "Coherence Properties of a Picosecond Dye Laser Oscillator Amplifier", Meeting of the Optical Society of America, Symposium on Ultrafast Photophysics, Paper Tu G4, October 1984.

5. J.-C. Diels, J. J. Fontaine, I. C. McMichael, and F. Simoni, "Control and Measurement of Ultrashort Pulse Shapes (in Amplitude and Phase) with Femtosecond Accuracy", Applied Optics **24**, 1270-1282 (1985).

6. C. R. Vidal and J. Cooper, "Heat-pipe Oven: A new, well defined metal vapor device fort spectroscopic measurements", J. of Applied Phys. **40**, 3370-3374 (1969).

7. J.-C. Diels, E. W. Van Stryland, and G. Benedict, "Design and Test of a Device for Measuring Pulse Durations Between 0.1 and 100 ps", CLEOS, TuII5 (February 1978); "Generation and Measurements of Pulses of 0.2 psec Duration", Optics Comm. 25, 93 (1978).

8. J.-C. Diels, "Coherent propagation and Harmonic generation", 6^{th} Vavilov Conference on Coherence and Nonlinear Optics, Novosibirsk, June 1979, Proceedings Vol 1, 206 (1979).

9. W. Dietel, J. J. Fontaine, and J.-C. Diels, "Intracavity Pulse Compression with Glass: A New Method of Generating Pulses Shorter than 60 Femtoseconds", Optics Letters **8**, 4 (1983); J. J. Fontaine, W. Dietel, and J.-C. Diels, "Chirp in a Mode-Locked Ring Dye Laser", IEEE Journal of Quantum Electronics, **QE-19**, 1467 (October 1983).

10. J.-C. Diels, H. Vanherzeele, and R. Torti, "Femtosecond Pulse Generation in a Linear Cavity Terminated by an Anti-resonant Ring", Conf. on Lasers and Electro-optics, Paper WC5, Anaheim, California (June 1984); H. Vanherzeele, J.-C. Diels, and R. Torti, "Tunable Passive Colliding Pulse Mode-Locking in a Linear Dye Laser" Optics Letters, **9**, 549-551 (1984).

11. H. Vanherzeele, R. Torti and J.-C. Diels, "Synchronously Pumped Dye Laser Passively Mode-Locked with an Antiresonant Ring", Applied Optics, **23**, 4182-4183 (1984).

12. J.-C. Diels, N. Jamasbi, and L. Sarger, "Engineering of a Five Mirror Femtosecond Laser, Using Geometrical Astigmatism Compensation", CLEO 86, San Francisco (june 1986); J.-C. Diels, N. Jamasbi, and L. Sarger, "Design of a 50 fsec Linear Laser and Analysis of the Colliding Pulse Effect", Int. Conf. on Ultrafast Phenomena, Snowmass, june 1986.

13. J.-C. Diels and J. Stone, "Multiphoton Ionization Under Sequential Excitation by Coherent Pulses", Physical Review **A 31**, 2397-2402 (1984).

14. J.-C. Diels and I. C. McMichael, "Spectroscopic Techniques in the Femtosecond Time Scale", Proceedings of the First International Laser Science Conference, Dallas (TX) (1985).

15. J.-C. Diels and S. Besnainou, "Multiphoton Coherent Excitation of Molecules", submitted to J. Chem. Phys (1986).

VIII. **PERSONNEL**

Dr. J.-C. Diels, Principal investigator.

Dr. H. Vanherzeele, Post Graduate Research Scientist.

Mr. D. Ussery, Research Associate.

Mr. Anadi Mukherjee, Research Assistant.

Mrs. Nandini Mukherjee, Research Assistant.

IX. **PUBLICATIONS UNDER GRANT AFOSR-82-0332**

1. H. Vanherzeele, H. J. Mackey, and J.-C. Diels, "Spatial and Temporal Properties of a Tunable Picosecond Dye Laser Oscillator-Amplifier System", Applied Optics **23**, 2056-2061 (1984).

2. H. Vanherzeele and J.-C. Diels, "Coherence Properties of a Picosecond Dye Laser Oscillator Amplifier", Meeting of the Optical Society of America, Symposium on Ultrafast Photophysics, Paper Tu G4, October 1984.

3. J.-C. Diels and J. Stone, "Multiphoton Ionization Under Sequential Excitation by Coherent Pulses", Physical Review **A 31**, 2397-2402 (1984).

4. J.-C. Diels, H. Vanherzeele, and I. C. McMichael, "Investigation of Multiphoton Coherent Excitation by Pulsed Sequences", Laser´s 84, Nov 1984 (invited).

5. J.-C. Diels and J. Stone, Laser´s 82, New Orleans, December 1982.

6. J.-C. Diels and H. Vanherzeele, "Picosecond Pulse Multiphoton Coherent Propagation in Vapors", Ultrafast Phenomena, Proceedings edited by D. H. Auston and K. B. Eisenthal, pp 233-235, Springer, Berlin (1984).

7. "Coherent Multiphoton Interactions using Sequences of Picosecond Pulses", A. Mukherjee, N. Mukherjee, G. Arzumanyan, and J.-C. Diels, Int. Quantum Electronics Conf., San Francisco (june 1986).

8. "Coherent Multiphoton Resonant Propagation and Harmonic Generation in Metal Vapors", A. Mukherjee, N. Mukherjee, G. Arzumanyan and J.-C. Diels, Int. Conf. on Ultrafast Phenomena, Snowmass, june 1986.

APPENDIX A

Reprinted from Applied Optics, Vol. 23, page 2056, July 1, 1984

Spatial and temporal properties of a tunable picosecond dye-laser oscillator–amplifier system

Herman Vanherzeele, H. J. Mackey, and J.-C. Diels

In this paper, we describe a high-power picosecond dye-laser system providing tunable 1.5-mJ pulses with a uniform wave front and Gaussian spatial profile. With the aid of a computer controlled data acquisition system, we have analyzed for the first time the temporal coherence properties of such a system.

I. Introduction

We report the development of a picosecond pulse dye-laser oscillator–amplifier system designed for experiments of resonant coherent propagation.[1] Such experiments put stringent requirements on the properties of the laser system, most of which will be reviewed briefly in Sec. II. We have been able to meet these requirements using a commercially available synchronously pumped dye laser in combination with a home-built amplifier. As we will explain in Sec. III, this amplifier consists of three stages being pumped by a frequency-doubled Nd:YAG laser. The first two stages are pumped transversely, while the last stage is pumped longitudinally. We suceeded in achieving a high gain, while avoiding a buildup of amplified spontaneous emission (ASE), without the use of spatial filters or saturable absorbers. Accurate synchronization of the various pulses combined with a careful optimization of the pump and amplified beam geometry ensures that the energy of the pump is channeled into the picosecond pulse rather than into ASE. Compared with purely longitudinally pumped systems, our transverse-longitudinal pumping geometry combines the advantage of a higher output energy with the ability to control the spatial beam profile. In Sec. IV, we will present interferometric autocorrelation measurements[2,3] performed for the first time on such a picosecond pulse dye-laser oscillator–amplifier system. These measurements, for which a new kind of data acquisition system needed to be developed, show that our amplifier does not significantly change the temporal properties of the dye-laser pulses. Preliminary measurements of coherent two-photon absorption in lithium demonstrate that this system meets the stringent coherence requirements of a multiphoton coherent propagation experiment.

II. General Design Considerations for a Picosecond Pulse Dye Amplifier

Even though we designed our amplifier for achieving a particular goal (saturation of the 2s–4s transition of lithium at 571.2 nm), the main specifications are desirable requirements for a large number of experiments: (1) high output energy; (2) minimum ASE; (3) good beam quality for interferometric experiments, i.e., uniform beam profile and flat distortion-free wave fronts; (4) no temporal phase-modulation effects; (5) both short- (pulse-to-pulse) and long-term stability; (6) availability of a cw pilot beam propagating through the system for the ease of alignment of the target experiment. Each requirement dictated one or more basic design features of the amplifier to be built as we will explain now. (See, e.g., Refs. 4 and 5 and additional references therein for a theoretical analysis.)

Obviously, a high output energy calls for an optimum use of the pump radiation, which in turn requires the minimum beam diameter in each amplifier stage compatible with a maximum unsaturated gain. Maximizing the gain for a given input also requires minimization of ASE. This can be achieved through (1) accurate timing of the pump pulse relative to the picosecond pulse to be amplified in each stage, thereby minimizing the overlap between the gain pulse in one cell and the ASE from the adjacent cell; (2) accurate geometrical matching of the pump beam and the picosecond dye-laser beam to maximize uniform pump depletion by the latter in each cell; (3) appropriate choice of dyes. The choice of dyes is further limited by our requirement that the system should be transparent for the unamplified dye-laser pulses, which serve as a cw pilot beam. This last con-

The authors are with North Texas State University, Center for Applied Quantum Electronics, Physics Department, Denton, Texas 76203.

Received 16 November 1983.
0003-6935/84/132056-09$02.00/0.

dition is particularly important in applications which require a critical alignment of the amplified beam. For our applications, the dye-laser beam is sent first along the axis of an interferometric delay line and subsequently through a long but narrow heat pipe, an operation that requires a cw beam. The requirement of an aberration-free temporal and spatial beam profile imposes the following design features: (1) short dye cells to minimize pulse-broadening and phase-modulation effects due to the solvent[6,7]; (2) the absence of filters and saturable absorbers to avoid wave front distortion in subsequent amplifiers; (3) a choice of solvents to obtain maximum thermal conductivity; (4) careful lateral adjustment of the pump beam in the longitudinally pumped cell to properly shape the spatial beam profile of the amplified dye-laser pulses. Finally, stability requirements put stringent conditions on the pump source for the amplifier: (1) short-term stability depends on the synchronization between dye laser and amplifier pump; (2) long-term stability merely imposes a constant thermal lens effect for the pump laser.

III. System Descriptions

The oscillator is a Spectra-Physics dye laser synchronously pumped by a Spectra-Physics Ar-ion laser actively mode locked at 82 MHz. For the gain medium we use rhodamine 6G in ethylene glycol (concentration 2×10^{-3} M). Although rhodamine 560 would yield a slightly higher gain at 571 nm, we prefer instead to use rhodamine 6G because of its better chemical stability. (The rhodamine 560 solution has to be replaced every week.) Wavelength tuning ~571 nm is achieved with a three-plate birefringent filter. With a 30% output coupler, this sytem generates a continuous train of 3.6-nJ pulses with a duration of 6.2-psec FWHM.

Our three-stage dye amplifier sketched in Fig. 1 is pumped by a frequency-doubled Q-switched Nd:YAG oscillator-amplifier (Quanta Ray DCR-1). This system delivers 280-mJ pulses (530 nm) of 8-nsec FWHM at a repetition rate of 10 Hz. The polarization of this beam is orthogonal to the polarization of the dye-laser beam. Therefore, we put the longitudinally pumped stage between crossed polarizers to couple out both the amplified dye-laser beam and the remaining part of the pump beam. A 1.5-m optical delay separates the dye-laser oscillator from the first amplifying cell to prevent oscillation of the latter with the output mirror of the former.

A. Beam Geometry

To prevent ASE from building up between stages, a direct vision prism is inserted between the first and second stages. This is the sole optical isolator used in our amplifier, in contrast to other systems which need, in addition, saturable absorbers and pinholes.[4,5,9] Particularly important in this respect is the expanding beam geometry throughout the system not only to increase the effectiveness of the prism in discriminating against ASE but also to maximize the overall gain of the amplifier. Starting with a diameter of <1 mm in the first cell, the beam diameter is increased three times in the second cell and further expanded in the last stage. The latter is inserted between two lenses of a collimating beam expander with an aperture ratio of 5. This design configuration of the last stage serves a dual purpose. The expansion of the dye-laser beam is required to keep the energy density at 571 nm below the saturation energy density. On the other hand, the converging geometry of the pump beam is needed to maintain a sufficient level of excitation despite absorption in the dye. One should bear in mind that the performance limits of the dye-amplifier are defined in the last stage. Indeed, the saturation energy density over the output cross section of the last stage is the maximum energy per pulse that the system can deliver (e.g., 1 mJ/cm^2 for rhodamine 6G).[10] Because of its large cross section, this last stage requires most of the energy (77%) of the pump laser, while yielding only a low gain (factor 8). Of the remaining pump energy, 7% is used for the first stage (gain: 10^3) and 16% for the second stage (gain: 50).

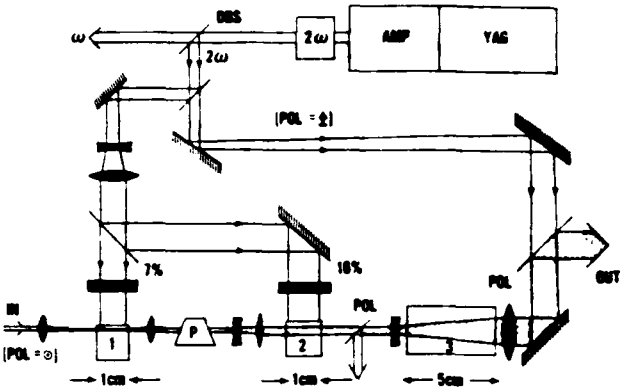

Fig. 1. Schematic representation of the three-stage amplifier (*DBS* = dichroic beam splitter, *POL* = polarizing beam splitter, *P* = direct vision prism).

B. Choice of Dyes

For the transversely pumped stages, we use 1-cm long flow through cells at Brewster incidence. The best dye candidate for a pump wavelength near 530 nm is rhodamine 6G (highest gain at 571 nm, longest lifetime). However, the absorption band of rhodamine 6G extends well beyond 571 nm. Therefore, rhodamine 560 has to be used in the first two stages (where the concentration is necessarily high) to obtain a reasonably large transmission of the unamplified dye-laser pulses through the system. It was determined empirically that the following dye combinations in the first and second cells yield the best results (maximum pump depletion, minimum ASE, and acceptable loss at 571 nm): for the first stage, a mixture of rhodamine 560 and rhodamine 6G in methanol (respectively, 2×10^{-3} M and 10^{-4} M); for the second stage, rhodamine 560 in methanol (10^{-3} M). Finally, for the last stage, which is 5 cm long, we use rhodamine 6G to fullly maximize the gain. The solvent in this stage is a 0.5% aqueous solution of Ammonix L.O. to minimize thermal effects. For the small dye concentration in this final stage (1.5×10^{-5} M), the absorption of the unamplified pulses is negligible.

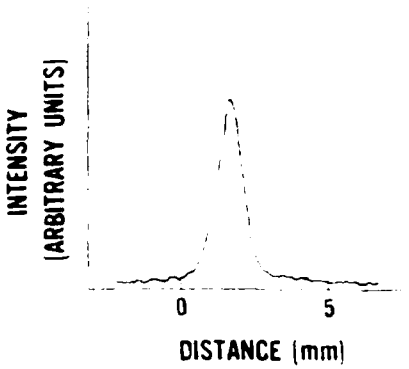

Fig. 2. Spatial profile of the amplified beam.

C. Synchronization

In Sec. II we emphasized the need for accurate and jitter-free synchronization in each stage between the pump pulse and the dye-laser pulse to be amplified. To reach this goal, we use the mode-locker drive of the Ar-ion laser as an absolute clock. Through direct digital division, this clock signal is scaled down to ~10 Hz. Next, this signal is used to interrogate the original clock signal in a logical AND gate thus providing a 10-Hz reference signal which is synchronized with the master clock (to within better than 0.5 nsec). A detailed description of the electronic circuit has been published elsewhere.[11] The 10-Hz reference in turn is used to directly trigger the Q-switch and, after an appropriate delay, also the flashlamps of the Nd:YAG oscillator-amplifier. The resulting jitter in the synchronization between the pump pulse and the dye-laser pulse to be amplified is of the order of 1 nsec.

To further minimize energy fluctuations of the amplified pulse due to this small remaining jitter, we synchronize the first stage at the leading edge of the pump pulse, while the second stage is synchronized at the trailing edge. This procedure further helps in reducing undesirable coupling in ASE between the initial stages.

D. Performance of the System

The output energy of our amplifier is ~1.5 mJ/pulse. Pulse-to-pulse stability is better than 20%. This is a good result for a chain of amplifiers, none of which is saturated. Using fresh dyes, the long-term stability is also good (5% over a period of 10 h). For an optimum synchronization, the ratio of ASE energy to pulse energy after the last stage is only a few percent.

The spatial intensity distribution of the amplified beam has also been examined using an optical multichannel analyzer (OMA). Because the first two stages are pumped transversely, one does not expect a uniform gain profile through the whole chain. Therefore, one may fear that the amplifier design may not provide a useful and smooth pulse spatial profile. Our measurements instead have shown that, by carefully positioning the pump beams relative to the amplified beam in the last two stages, we can achieve complete control of the profile of the output beam. An example is shown in Fig. 2. With the OMA in the free-running mode, no shot-to-shot variations of this profile were detected.

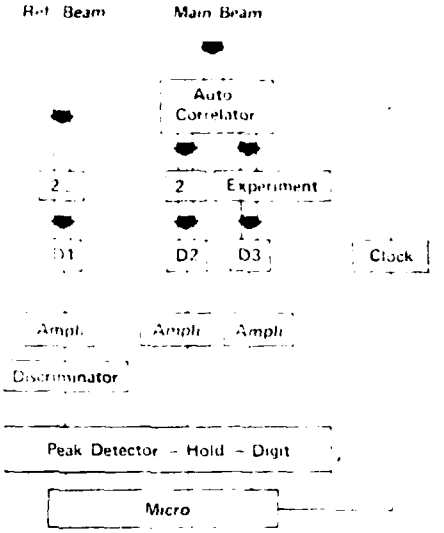

Fig. 3. Data acquisition system: hardware.

The quality of the amplifier output was also examined with a Mach-Zehnder interferometer. Complete extinction of the beam over its entire cross section could be achieved with the interferometer balanced. This demonstrates the absence of wave front distortion in the amplifier chain.

IV. Temporal Properties of the Amplified Pulses

Equally important for coherent propagation experiments are the temporal properties of the amplified pulses. We infer these properties from second-order intensity and fringe-resolved autocorrelation measurements using a Mach-Zehnder interferometer.[2,3] The main difficulty involved in these measurements stems from the fact that the delay arm of the interferometer has to be moved uniformly with absolute subwavelength accuracy over a sufficiently long distance. Indeed, the requirement that the motion of the delay arm be continuous without the discontinuities that would result from the static friction coefficient (being larger than the dynamic one) implies a minimum scanning speed. On the other hand, however, an upper limit for this scanning speed is set by the repetition rate of the amplifier (10 Hz) and the requirement that there be at least twenty to thirty data points per period to resolve individual fringes. Obviously, both requirements are conflicting. Moreover, the remaining pulse-to-pulse instabilities will cause large fluctuations on top of second-order fringes, thereby washing out the fringe contrast. Averaging out the data over a large number of laser shots will only further reduce this contrast. To solve these problems, we had to develop an adequate data acquisition system.

A. Data Acquisition System

The hardware of our data acquisition system is schematically represented in Fig. 3. About 1% of the amplifier output is used as a reference beam, the remaining part is sent through the interferometer. Both

the reference beam and one of the output beams of the interferometer are frequency doubled and digitized after detection by photoconductive PIN diodes (UDT 100L). The other output beam of the interferometer is used for two-photon coherent propagation experiments in lithium vapor. The electronic discriminator in the reference channel rejects pulses with either too low or too high UV energy. This is an essential feature for our coherent two-photon propagation experiments in lithium vapor which depend critically on the pulse energy (through induced Stark shifts).

The aforementioned problem of smoothing the interference fringes is solved in the software of our data acquisition system. First, errors due to amplitude fluctuations of the pulses are reduced to a few percent by computing the ratio of the signals in channels 2 and 1. Next, while varying the delay in the autocorrelator at a regular speed of 0.16 μm/sec, the resulting fringes are partitioned over a large number of sets (each set typically has 100 fringes). Per set, two different averaging processes are performed. On the one hand, all data in each set are averaged thereby washing out the fringes completely. For a large number of sets this will yield the conventional 3:1 intensity autocorrelation curve. On the other hand, an average fringe per set is constructed by averaging the data in a single periodicity over the whole set. An example is shown in Fig. 4. This averaging process permits one to keep track of small phase shifts over consecutive sets of fringes. For a large number of sets, it yields the fringe-resolved 8:1 autocorrelation curve. In this way one obtains both autocorrelation curves during a single experiment.

B. Data Reduction

By fitting the experimental data for both the intensity and the fringe-resolved autocorrelation curves, it is possible to determine accurately the temporal properties of the amplified pulses. From the experimental arrangement described above, we obtain two recordings of second harmonic signal vs delay: the intensity and the interferometric autocorrelation. The intensity autocorrelation curve provides a first estimate of a reasonable pulse shape and pulse duration which is used as a starting point in attempting to fit the interferometric autocorrelation measurements. For a given trial function for the complex electric field envelope

$$\tilde{E}(t) = E(t)\exp[i\phi(t)], \tag{1}$$

a numerical computation is made of the interferometric second-order autocorrelation

$$F(\tau) = \frac{\int_{-\infty}^{\infty}|\tilde{E}(t) + \tilde{E}(t-\tau)\exp(-2\pi i\nu\tau)|^4 dt}{2\int_{-\infty}^{\infty}|\tilde{E}(t)|^4 dt} \tag{2}$$

of which the intensity autocorrelation $I(\tau)$ is the subpart excluding the rapidly varying terms in $\cos(2\pi\nu\tau)$ and $\cos(4\pi\nu\tau)$ of Eq. (2):

$$I(\tau) = \frac{1}{2} + \frac{2\int E(t)E(t-\tau)dt}{\int E^2(t)dt}. \tag{3}$$

The computations are organized as follows: first, at $\tau = 0$ and at $\tau = 1/2\nu$ the first-fringe maximum and minimum are computed; subsequently τ is incremented by $\Delta\tau = 1/\nu$ to generate the next pair of points and so on. To improve the accuracy, an additional loop generates near each fringe-maximum three points of $F(\tau)$, not more than two of them being located at the same side of that maximum. With a parabolic fit through these points, the computer determines (1) the true location of maximum (τ_{max}), (2) the correct $\Delta\tau$, which will be used to initiate the next main loop, (3) the location of the fringe-minimum (τ_{min}), and finally (4) the corresponding values of $F(\tau_{max})$, $F(\tau_{min})$, and $I(\tau_{max})$. Once $I(\tau)$ and both envelopes of $F(\tau)$ are computed in this way, the pulse parameters (shape, asymmetry, width, and chirp) are adjusted until a good fit with the experimental data can be reached. Finally, for the best fitting pulse, the deviation of the average frequency

$$\langle\nu\rangle = \frac{\int \nu(t)E^2(t)dt}{\int E^2(t)dt} \tag{4}$$

and the pulse bandwidth[12]

$$\Delta\nu = \sqrt{\frac{\int \nu^2(t)E^2(t)dt}{\int E^2(t)dt} - \langle\nu(t)\rangle^2 + \frac{\int \dot{E}^2(t)dt}{\int E^2(t)dt}} \tag{5}$$

are obtained.

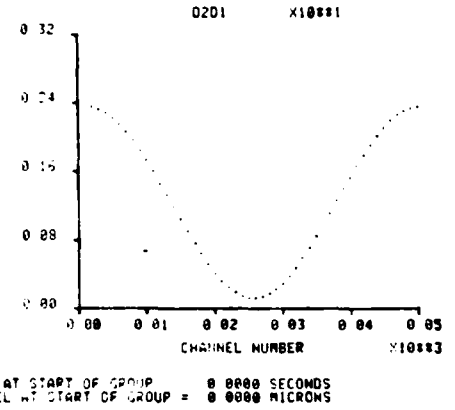

Fig. 4. Example of an average fringe representing a set of fringes.

C. Results: Pulse Characteristics Before and After Amplification

Figure 5(a) shows the intensity autocorrelation curve for the amplified pulses (dashed line). The solid line represents a numerical fit using a Gaussian pulse shape with 6.2-psec FWHM [i.e., 5.27-psec HW$(1/e^2)M$]. Note that an intensity autocorrelation cannot effectively distinguish between a Gaussian and a sech pulse shape.

From Eq. (3), it is clear that the intensity autocorrelation is phase independent and, therefore, does not carry any information about the pulse chirp. On the other hand, as shown in Refs. 2 and 3, the interferometric autocorrelation is sensitive to the pulse chirp $\phi(t)$. The experimental results obtained for the latter with our amplified pulses are shown in Fig. 5(b) (dashed line). The solid line in Fig. 5(b) represents again the best theoretical fit: Gaussian pulses (6.2-psec FWHM) with a phase modulation proportional to the pulse intensity ($\phi = 1.43\,E^2$). For comparison, the 8:1 auto-

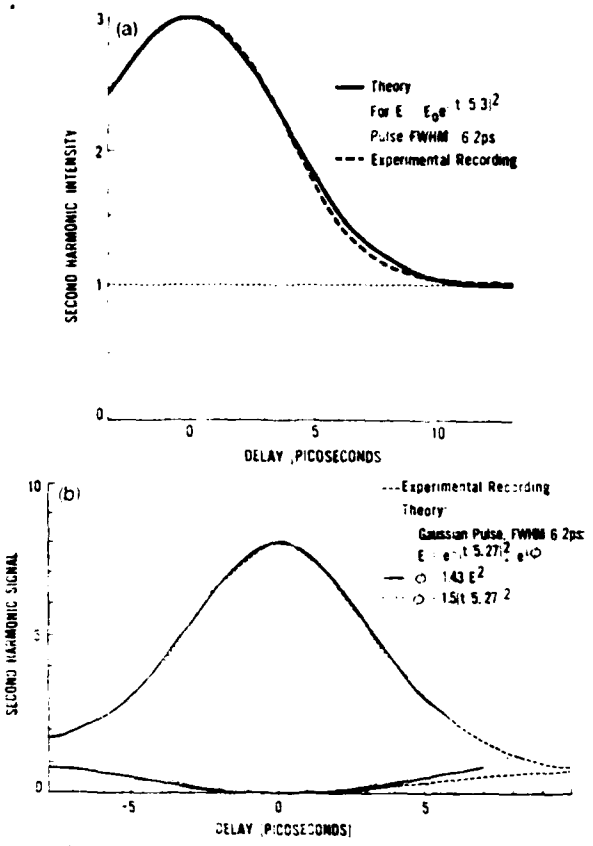

Fig. 5. Experimental results and best theoretical fits for (a) the intensity autocorrelation curve and (b) the fringe-resolved autocorrelation curve [dashed lines are experimental curves, solid lines represent the theoretical fits; for the dotted line in (b), see text].

correlation curve for the same Gaussian pulses but having instead a linear phase modulation [best fit: $\phi = 1.5\,(t/5.27)^2$] is also shown in Fig. 5(b) (dotted line). The data imply that the amplified pulses are not completely bandwidth limited; according to Eq. (5), the bandwidth is 79 GHz.

The data shown in Fig. 5(b) are much more sensitive to phase-modulation effects than, e.g., spectral data. The bandwidth duration product for the nonlinear chirped pulses in our case is 0.49 or only 10% larger than the minimum of 0.44 for unchirped Gaussian pulses. On the other hand, the FWHM of the upper envelope of the interferometric autocorrelation curve for our pulses is 7.2 psec compared with 9.5 psec for unchirped pulses; the lower envelope is even more sensitive to phase-modulation effects: its FWHM changes by almost 50% from our chirped pulses (9.5 psec) to the case of unchirped pulses (14.7 psec).

The kind of chirp we have detected for the amplified pulses, i.e., a chirp proportional to the time derivative of the pulse intensity, is typical of self-phase modulation of the pulses. An interferometric autocorrelation of the unamplified dye-laser pulses as shown in Fig. 6 clearly indicates that the origin of the chirp is in the laser oscillator rather than in the amplifier chain. Partial chirp compensation is taking place in the amplifier: the interferometric autocorrelation curve for the unamplified

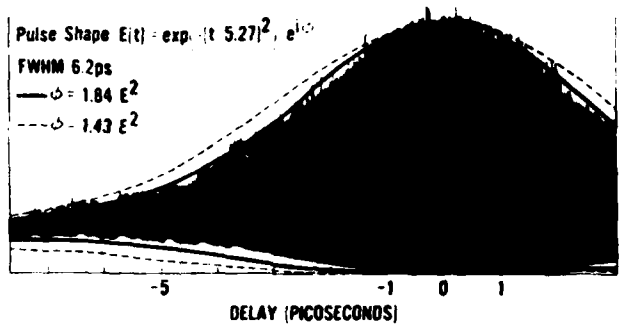

Fig. 6. Interferometric autocorrelation curve for the unamplified pulses (the solid line represents the best fit; the dashed line corresponds to the best fit for the amplified pulses).

pulses reveals a phase modulation proportional to 1.84 E^2 (rather than 1.43 E^2 for the amplified pulses).

To conclude, our interferometric autocorrelation measurements as shown in Fig. 5(b) have demonstrated that the phase distortion introduced by the amplifier is small in the time as well as in the space domain. A peak-to-background of 8:1 can only be obtained with spatially coherent pulses. Indeed, at zero delay, the maximum signal of eight times the background requires that the two halves of the pulse interfere constructively over their entire cross section.

V. Conclusions

In summary, we have developed a picosecond pulse dye-laser oscillator–amplifier system tunable near 570 nm. At a repetition rate of 10 Hz the output consists of 1.5-mJ pulses. Both the short- and long-term stability are excellent. Contrary to other similar systems, we have avoided the use of either pinholes or saturable absorbers. Therefore, our system requires fewer components, which makes the alignment easier. Despite the absence of pinholes and saturable absorbers, the ratio of ASE energy to pulse energy after the last stage is only a few percent. An additional advantage of our system over other short pulse amplifiers is that the unamplified dye-laser pulses are transmitted through the system thus providing a cw pilot beam. This is an important feature for applications requiring a critical alignment. Our amplifier output has a uniform spatial beam profile and distortion-free wave fronts. The temporal properties of the amplified pulses have also been investigated using a computerized data acquisition system specially developed for this purpose. The pulses are Gaussian (FWHM: 6.2 psec) and present a nonlinear chirp (1.4 E^2). The bandwidth is 79 GHz. It was shown that the origin of the chirp is in the dye-laser oscillator, rather than in the amplifier chain.

The authors would like to acknowledge the valuable assistance of D. Maxson, who interfaced the detection system to the microprocessor. H. Vanherzeele is on leave from the University of Brussels; he acknowledges financial support from the NFWO for travel expenses. This research was supported by AFOSR under contract 82-0332.

References

1. J.-C. Diels and A. T. Georges, "Coherent Two-Photon Resonant Third- and Fifth-Harmonic Vacuum-Ultraviolet Generation in Metal Vapors," Phys. Rev. A **19,** 1589 (1979).
2. J.-C. Diels, E. W. Van Stryland, and D. Gold, in *Picosecond Phenomena*, C. V. Shank, S. L. Shapiro, and E. P. Ippen, Eds. (Springer, New York, 1978), p. 117.
3. J.-C. Diels, I. C. McMichael, J. J. Fontaine, and C. Y. Wang, in Proceedings, *Third International Conference on Picosecond Phenomena* (Springer, Berlin, 1982), p. 116.
4. A. Migus, C. V. Shank, E. Ippen, and R. L. Fork, "Amplification of Subpicosecond Optical Pulses: Theory and Experiment," IEEE J. Quantum Electron. **QE-18,** 101 (1982).
5. G. Haag, M. Munz, and G. Marowsky, "Amplified Spontaneous Emission in Laser Oscillators and Amplifiers," IEEE J. Quantum Electron. **QE-19,** 1149 (1983).
6. Y. Ishida, K. Naganuma, and T. Yajima, in *Technical Digest, Conference on Lasers and Electrooptic Systems* (Optical Society of America, Washington, D.C., 1983), paper ThQ2.
7. W. Dietel, J. J. Fontaine, and J.-C. Diels, "Intracavity Pulse Compression with Glass: A New Method of Generating Pulses Shorter than 60 fsec," Opt. Lett. **8,** 4 (1983).
8. J. L. Martin, R. Astier, A. Antonetti, C. A. Minard, and A. Orszag, "Amplification des Impulsions Subpicosecondes d'un Laser à Colorant et Génération d'un Continuum," C. R. Acad. Sci. **289,** 45 (1979).
9. R. L. Fork, C. V. Shank, and R. T. Yen, "Amplification of 70-fs Optical Pulses to Gigawatt Powers," Appl. Phys. Lett. **41,** 223 (1982).
10. P. Hammond, "Comparison of Experimental and Theoretical Excited State Spectra for Rhodamine 6G," IEEE J. Quantum Electron. **QE-16,** 1157 (1980).
11. J. Menders and J.-C. Diels, "Accurate Scaling of rf Frequencies to a Few Hz," Rev. Sci. Instrum. **53,** 1093 (1983).
12. J. C. Diels and E. L. Hahn, "Carrier-Frequency Distance Dependence of a Pulse Propagating in a Two-Level System," Phys. Rev. A **8,** 1084 (1973).

APPENDIX B

FOUR PHOTON RESONANT COHERENT INTERACTION

We consider an atomic system excited by a coherent electromagnetic pulse which is in condition of four photon resonance between the ground state $|1\rangle$ and a state $|2\rangle$. The 6^1S_0 - 6^1D_2 transition of mercury will be used as a numerical example. The calculations for the 6s - 7s transition are slightly simpler, since the energy of a single photon is not sufficient to make transitions from the upper level (7s) to the continuum.

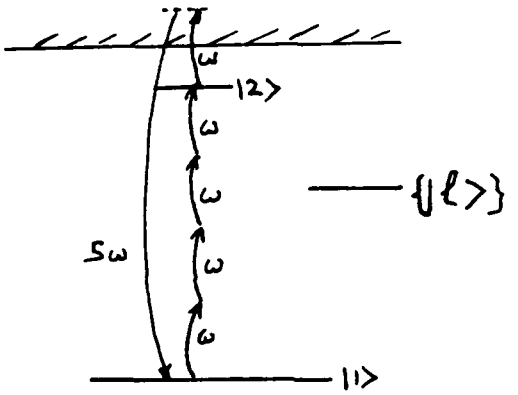

Let us designate by $\{|\ell\rangle\}$ the set of states that are coupled to $|1\rangle$ or $|2\rangle$ by dipole moments. It is postulated that no other transition than $|1\rangle$ - $|2\rangle$ is resonant with the applied field. The adiabatic approximation can be used to solve the equations of motion for the elements of the density matrix connecting a state $|\ell\rangle$ to the level $|1\rangle$ ($\rho_{1\ell}$) of $|2\rangle$ ($\rho_{2\ell}$). The case of the state $|\ell\rangle$ in the continuum has to be treated differently, since the transition $|2\rangle$ - $|\ell\rangle$ can then be considered to be exactly resonant. A perturbation treatment is used in that case, justified by the weakness of the bound-free matrix elements. It should be noted however that the latter approximation has never been tested in the femtosecond range, and that experiments will be made to test this particular aspect of the model.

The linearly polarized electromagnetic pulse is described by the electric field vector:

$$\mathbf{E} = E(t)e^{i\omega t} + c.c. \tag{1}$$

where E(t) is the slowly varying complex amplitude of the field. The equations of motion for the density matrix:

$$\frac{\partial \boldsymbol{\rho}}{\partial t} = \frac{i}{\hbar}[\boldsymbol{\rho}, H] \tag{2}$$

can be solved by adiabatic approximation for the density matrix elements involving the levels $|\ell>$, essentially reducing the description of the atomic system to that of a two-level system:

$$\frac{\partial \sigma_{12}}{\partial t} = (-i\Delta\omega - \frac{\gamma_2}{2} - \frac{1}{T_2})\sigma_{12} + i\{\frac{E}{\hbar}\}^4 r_{12}(\sigma_{22} - \sigma_{11}) \tag{3}$$

$$\frac{\partial \sigma_{22}}{\partial t} = (-\frac{1}{T_1} - \gamma_2)\sigma_{12} - 2\,\mathrm{Im}[\{\frac{E^*}{\hbar}\}^4 r_{12}\,\sigma_{12}] \tag{4}$$

$$\frac{\partial \sigma_{11}}{\partial t} = 2\,\mathrm{Im}[\{\frac{E^*}{\hbar}\}^4 r_{12}\,\sigma_{12}] \tag{5}$$

In Eqs (3) - (5), σ_{ij} are the slowly varying amplitudes of the density matrix elements. The transition matrix element responsible for four photon absorption is:

$$r_{12} = -\sum_{\substack{\ell \neq 1,2 \\ k \neq 1,2,\ell \\ f \neq 1,2,k}} \frac{\mu_{1f}\,\mu_{fk}\,\mu_{k\ell}\,\mu_{\ell 2}}{(3\omega - \omega_{\ell 1})(2\omega - \omega_{k1})(\omega - \omega_{f1})} \tag{6}$$

In the case of the 6s - 6d transition of mercury:

$$r_{12} = -2.03\ 10^{-162}(C\cdot m)^4 s^3$$

The detuning is defined as:

$$\Delta\omega = 4\omega - \omega_{21} - \delta\omega_{21} \tag{7}$$

where we include a quadratic Stark shift of the 4-photon resonance:

$$\delta\omega_{21} = \frac{1}{\hbar}[\alpha'_1(\omega) - \alpha'_2(\omega)]|E|^2 \tag{8}$$

In Eq. (8), $\alpha'_i(\omega)$ is the real part of the polarizability of the state $|i\rangle$ at the frequency ω. The complex polarizability of $|1\rangle$ or $|2\rangle$ is given by:

$$\alpha_i(\omega) = \frac{1}{h}\sum_{\ell}\left[\frac{1}{(\omega_{\ell i} + \omega)} + \frac{1}{(\omega_{\ell i} - \omega)}\right]|\mu_{\ell i}|^2 \tag{9}$$

The proximity of the 6p level resonantly enhances the second term of the polarizability for level $|2\rangle$ in the case of the 6s - 6d transition. The values for that transition are:

$$\alpha_1(\omega) = 4.7\ 10^{-40}\ [\text{MKS}] \tag{10}$$

$$\alpha_2(\omega) = 5.3\ 10^{-39} - i\ 7.2\ 10^{-40}\ [\text{MKS}] \tag{11}$$

The imaginary part of the polarizability of state $|2\rangle$ accounts for the ionization rate from the upper state (in Eqs. (3) and (4)):

$$\gamma_2 = \frac{2\alpha''_2(\omega)}{\hbar}|E|^2 \tag{12}$$

The calculation of the time dependent macroscopic polarizations at the various frequencies is straightforward but tedious, because of the large number of terms involved. For instance, in the calculation of the polarization at ω, one has to include intensity dependent one-photon polarizabilities of the form $|E|^2\sigma_{22}E$; $|E|^2\sigma_{11}E$; $|E^*|^3\sigma_{12}$, in addition to the term in $\alpha_i\,\sigma_{ii}E$ that appeared already in the two-photon calculations [1]. In the case of the 6s - 6d transition of mercury, the polarization at ω reduces to:

$$P_1 = [\alpha_1(\omega)\sigma_{11}+\alpha_2(\omega)\sigma_{22}]E + 2r_{12}(\frac{E^*}{\hbar})^3\sigma_{12} + .003\frac{r_{12}|E|^2E\sigma_{11}}{\hbar^3}$$

The polarizations have been calculated at the various frequencies, and inserted in Maxwell's equations, to compute numerically the propagation of the various fields and the conversion efficiencies. The case of the 6s - 6d transition is particularly complex because of the large Stark shift. In addition, ionization from the upper level tends to wash out all coherent interaction effects, except for the shortest pulses, for which the validity of our model has to be tested.

The 6s - 7s transition appears to be an ideal candidate for efficient fifth harmonic generation. The proximity of a 9p level near the fifth harmonic frequency accounts for a resonant enhancement of the fifth harmonic generation. Low loss propagation of properly phased pairs of pulses is made possible by the absence of single photon photoionization from the upper level (7s) and the reduced Stark shift of the resonant transition.

APPENDIX C

DESIGN OF A 50 FSEC LINEAR LASER, AND ANALYSIS OF THE COLLIDING PULSE EFFECT.

Jean-Claude Diels, Nooshin Jamasbi
Center for Applied Quantum Electronics, P.O. Box 5368
North Texas State University,
Denton, Texas 76203. Ph (817) 565 3261.

and
Laurent Sarger
Centre de Physique Moléculaire Optique et Herzienne,
Université de Bordeaux I,
351 cours de la Libération, 33405 Talence, France.

An antiresonant (AR) ring has been proposed by Siegman [1] to obtain standing wave saturation in a linear mode-locked dye laser. This laser configuration is equivalent to that of a mode-locked ring laser if the saturable absorber is located at equal optical distance from the beam splitter (Fig. 1). Two technical problems seem to make this configuration impractical:

a) The requirement of tight focusing in the absorber [2, 3] implies a large beam size through the beam splitter, hence a large angle of the AR triangle, and a large astigmatism impeding the tight focusing.
b) It seems impractical to fulfill the "colliding pulse" condition for femtosecond pulses, since it requires to maintain equality of the two arms of the AR ring with an accuracy of 10 microns.

We demonstrate that the astigmatism of the AR ring (even for angles as large as 16 ^{o}) can be compensated by the geometry of the cavity (the astigmatism introduced by the other arm of the cavity can be used to compensate that of the antiresonant ring). Furthermore, this cavity configuration enables us to test for the first time experimentally the "colliding pulse" condition, independently of any other parameter. It is shown that the accuracy requirement for the equality of the two arms of the AR ring is much less stringent than anticipated. The operation of the laser is not affected by a departure from the "ideal" central position of less than 400 microns!

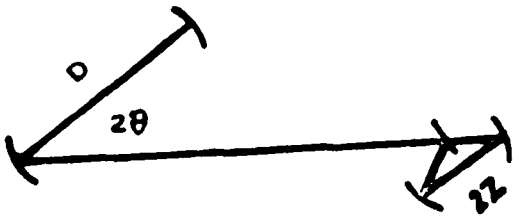

Figure 1: Sketch of the laser cavity.

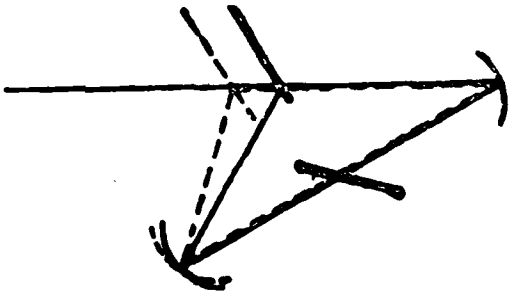

Figure 2: balancing the arms of the AR ring.

The laser cavity is simple enough to make a complete analytical ABCD matrix analysis possible (using the algebraic formula manipulation computer language "MACSYMA"). For any value of the angle θ, we compute the values of mirror spacing D and 2z that satisfy the stability criteria in the plane of the cavity and in the orthogonal plane. The resulting stability diagram shows "forbidden" ranges of angle θ for which no stable cavity can be designed (for instance, $13.5^{o} < \theta < 17^{o}$). Computation of the beam waists in the absorber indicate a large spot size (50 microns and more) for the first stability region. Astigmatism compensation is optimized in the small isolated stability range corresponding to $114 < D < 117$mm, for $21^{o} < \theta < 23^{o}$, where round spots a few microns in diameter are obtained. Because of the restricted dimensions of that stability region, the parameters of the laser cavity are accurately defined. For a given angle θ ($21^{o} < \theta < 23^{o}$), the beam waist (in the absorber) is a monotonous function of the mirror spacing D, making it possible to study the operation of the laser as a function of absorber saturation.

All the parameter (angles, mirror distances, positions of the images of the fluorescence spots) of the laser having been predetermined, the laser alignment follows a systematic and straightforward procedure. Using a 0.7 mm thick beam splitter, a very small amount of positive dispersion is needed to compensate the small phase modulation in the strongly saturated absorber dye, resulting in a stable mode-locked train of pulses as short as 50 fsec.

The "colliding pulse" effect can be investigated by changing the relative length of the two arms of the antiresonant ring, as sketched in Fig. 2. As the beam splitter is moved away from the position corresponding to the symmetric ring, the threshold pump power for short pulse operation remains constant in a 800 micron wide region. It is only for larger departures from the "equal arms" condition that this threshold power is seen to increase from 1.7 to 3.5 W. If the pump power is maintained at 3.5 W, none of the following parameters of the laser is affected by departing from the symmetric ring: the pulse output power, the intensity autocorrelation, and the losses of the antiresonant ring. Below the "threshold power for short pulse operation", the laser output consists in a train of long (psec) bursts of noise. It can be concluded that the "colliding pulse operation" is important in reducing the threshold for stable mode-locked operation, and in the formation stage of the steady state pulse from noise.

REFERENCES.

1. A. E. Siegman, "An antiresonant ring interferometer for coupled laser cavities, laser output coupling, mode-locking, and cavity dumping", IEEE J. Quantum Electron. QE-9, 247-250 (1973).
2. O. E. Martinez, R. L. Fork and J. P. Gordon, "Theory of passively mode-locked lasers including self-phase modulation and group velocity dispersion", Opt. Let. 9, 156-158 (1984).
3. J.-C. Diels, W. Dietel, J. J. Fontaine, W. Rudolph. and B. Wilhelmi, "Analysis of a mode-locked ring laser: chirped solitary-pulse solutions", Journal of the Opt. Soc. B, 2, 680-686 (1985).

DESIGN OF A 50 FSEC LINEAR LASER, AND ANALYSIS OF THE COLLIDING PULSE EFFECT.

SUPPORTING MATERIAL.

Analysis of existing femtosecond ring lasers led to a fairly complete understanding of the mechanisms of short pulse generation and compression in these lasers [1, 2]. Accurate diagnostic methods that have been developed confirmed details (pulse shape and phase modulation) of the theory [3]. It should thus be possible to design a laser based on that theory. Our main requirements are:

- a minimum number of intracavity elements;
- a cavity simple enough to make a complete parametric study possible;
- tight focusing in the absorber;
- standing wave saturation;
- an adjustable repetition rate.

Consistent with these requirements, we chose a linear laser cavity terminated by an antiresonant ring [4] (Fig. 1). Imposing a spot size of a few microns in the absorber results in a beam size of 4 mm on the focusing mirrors, therefore a minimum angle of incidence on these mirrors, hence a large astigmatism. The latter effect appears to conflict with the tight focusing requirement. Analytical calculations of the empty geometrical cavity show that the astigmatism at the absorber jet can be compensated by that at the amplifier arm. A stability diagram is plotted in Fig. 3, for radii of curvature of 7.5 cm at the amplifier jet, 3 cm at the absorber jet. No stable cavity can be designed for $13.5^{o} < \Theta < 17^{o}$. While the first stability region is very large, it is only at the edge of this region that a minimum beam waist (in the absorber) of 50 microns can be calculated. In the very small stability region corresponding to $114 < D < 117$ mm and $21^{o} < \Theta < 23^{o}$, the beam waists are circular, with a minimum diameter of a 4 microns. The calculation of the cavity is complemented by calculations of the size and shape of the beam in the amplifying jet. Because of the large astigmatism in that arm of the laser, the pumping geometry (focal distance of the argon laser focusing mirror and angle of incidence) is calculated to match the size and shape of the dye laser beam in the amplifier jet.

The (empty cavity) laser has a threshold of 400 mW (2% output coupling). With the saturable absorber, the laser exhibits the stable mode-locking behavior typical of ring lasers. The pulse duration has a sharp minimum of 50 fsec for an optimal amount of intracavity glass. However, iterative fitting [4] of the pulse spectrum (fig. 4a), the interferometric autocorrelation (fig. 4b) and the intensity autocorrelation (Fig. 4c) lead to an asymmetric pulse shape with a residual nonlinear phase modulation (in contrast to the measurements with the ring laser). It is therefore expected that even shorter pulses could be generated with this laser design, with a better match of the intracavity dispersion and phase modulation.

Since we observe that the two arms of the AR ring can be out of balance by as much as 0.8 mm, one may question the need for a "colliding pulse" configuration. For the case of astigmatism compensa-

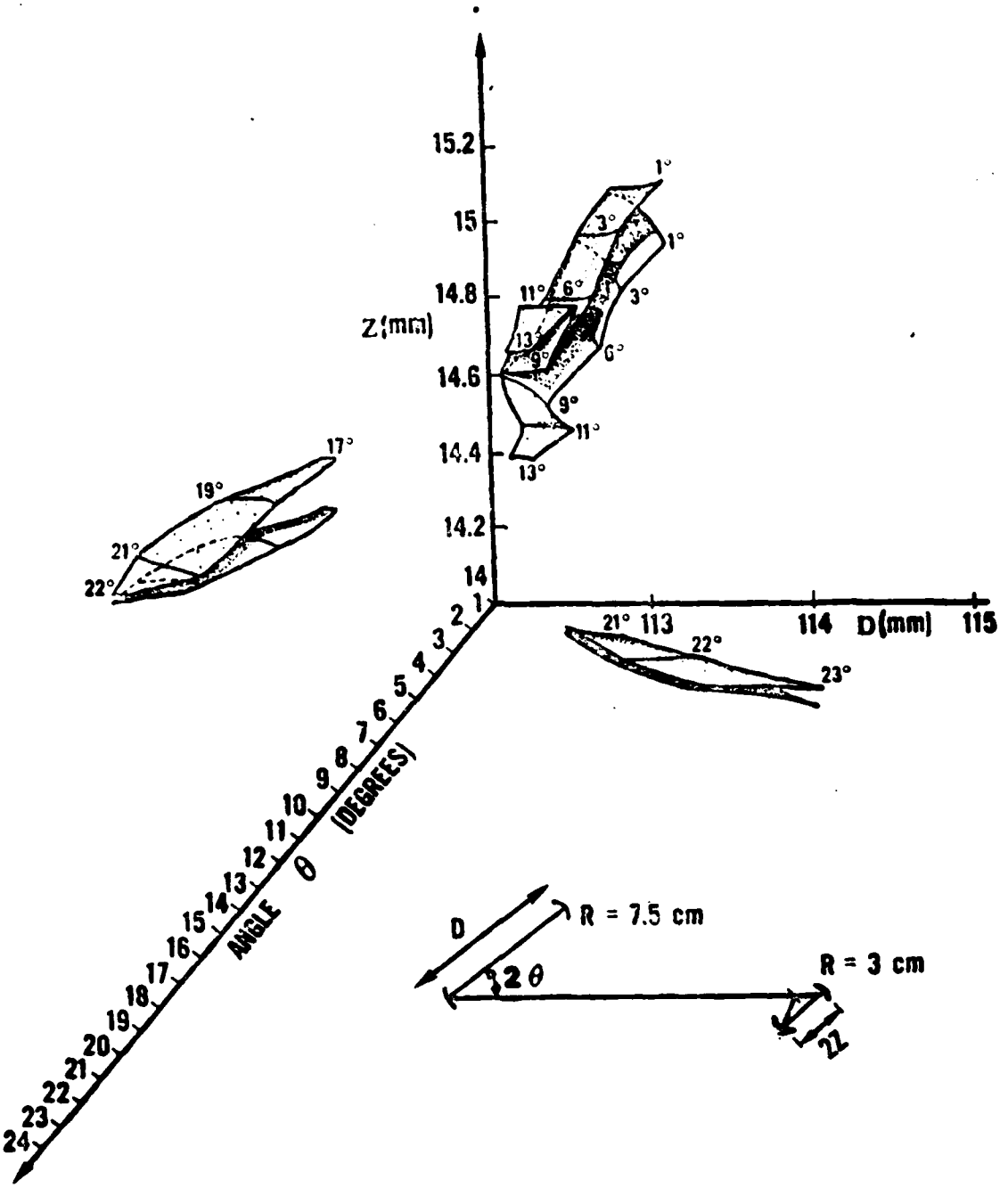

Figure 3: Stability Diagram.

tion at the absorber, the folded cavity obtained by removing the beam splitter (and adjusting z) is geometry identical to the AR ring cavity. Identical intensity autocorrelation traces are obtained with that cavity, which is essentially the same as that used over a decade ago 5. However, the stability is reduced, and the threshold a factor two higher.

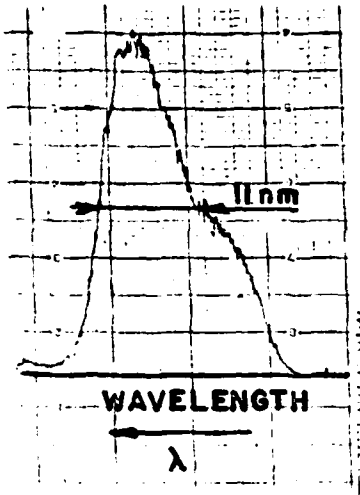

Figure 4a

Figure 4b

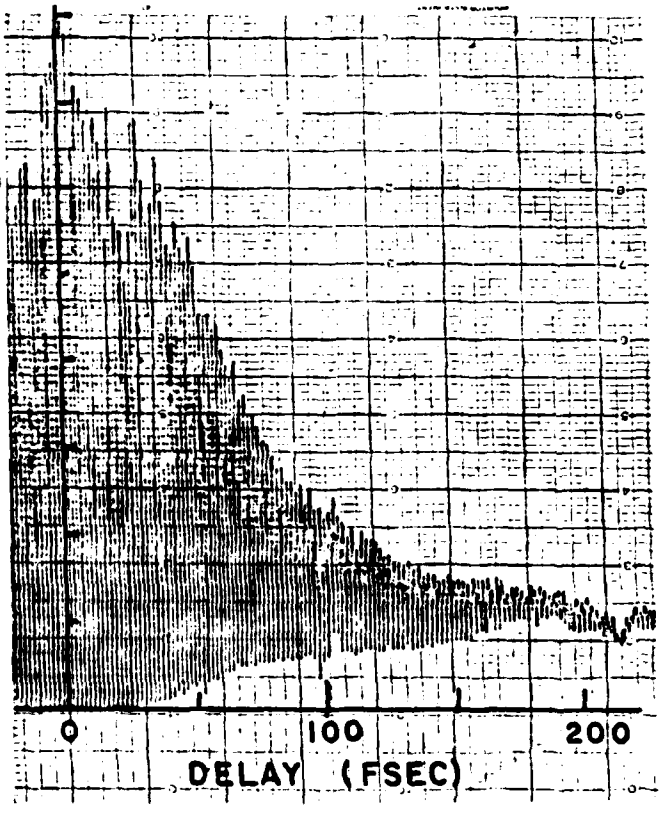

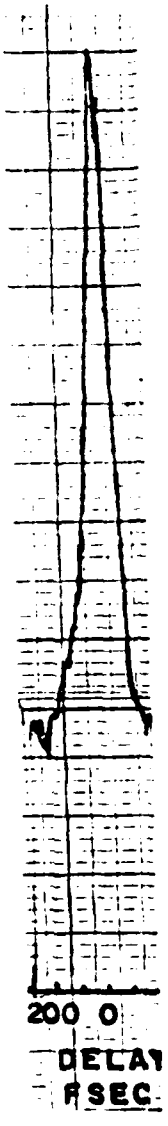

Figure 4c

In conclusion, we have successfully designed a laser cavity for which a straightforward, simple alignment procedure replaces the skills and artful expertise normally required for fsec lasers.

SUPPLEMENTAL REFERENCES.

4. J.-C. Diels, J. J. Fontaine, I.C. McMichael, and F. Simoni, "Control and measurement of ultrashort pulse shapes (in amplitude and phase) with fsec accuracy", Applied Optics 24, 1270-1282 (1985).
5. E. P. Ippen, C. V. Shank, A. Dienes, Appl. Phys. Lett. 21, 348-350 (1972).

APPENDIX D

PHYSICAL REVIEW A VOLUME 31, NUMBER 4 APRIL 1985

Multiphoton ionization under sequential excitation by coherent pulses

J.-C. Diels
Center for Applied Quantum Electronics, Department of Physics, North Texas State University, Denton, Texas 76203

J. Stone
Center for Laser Studies, University of Southern California, Los Angeles, California 90089-1112

(Received 14 August 1984)

The use of pulse sequences offers a solution to the conflicting requirements of spectral selectivity and high peak intensities needed to study multiphoton processes. In addition, it is shown that *random*—rather than regular—pulse sequences can provide unique information on the influence of coherence on a resonant multiphoton process, because the coherence can be adjusted independently of the resonance condition.

I. INTRODUCTION

Attention has been drawn in recent years to the possible use of pulse sequences to enhance quantum beat phenomena in molecules,[1] or to selectively enhance weak spectral lines.[2] Phase shifts in the light field for a single pair of pulses can be used to distinguish between single and multiphoton processes.[3] Statistically distributed phase switching on a cw field can give it the spectral and driving characteristics of a line-broadened source.[4] Here we discuss an application of pulse sequences in the area of laser-driven reactions. We choose as an example multiphoton ionization of atoms. However, the approach used here applies also to multiphoton dissociation of molecules—which has been the subject of extensive theoretical investigation[5]—or to any other process dependent on the absorption of several photons.

Two types of sequential excitation will be considered: deterministic and statistical. The motivation for using a sequence of identical pulses with a well-defined phase relationship is to combine the spectral selectivity offered by a regular pulse train with the high peak intensities of picosecond pulses, which are needed to excite higher-order processes.

A dimension of nonlinear mechanisms that is subject to experimental test is the coherence or lack of coherence in the process. But, as we discuss below, the single-pulse experiments that have been the mainstay of this area provide a fairly limited test of coherence. Multimode versus single-mode operation has been used[6,7] to vary the "coherence" of the laser source. This procedure has the disadvantage of varying the bandwidth—hence the resonance condition—simultaneously with the pulse coherence. We will show how a sequence of pulses of controlled phase can be used to vary the source coherence without affecting its central frequency or its spectral width.

By choosing the delays and phase between pulses to fit a chosen statistical distribution we can study how a multiphoton process is affected by those statistics. Such an approach, of averaging many measurements with a predetermined [illegible] of delays and phases to fit a given photon statistic), will be shown to have several advantages over other methods of studying the influence of source coherence on a multiphoton resonant process. As an illustrative example for the latter we have chosen multiphoton ionization in a metal vapor in the presence of a two-photon resonance.

II. THEORETICAL MODEL

We consider an atomic system in conditions of two-photon resonance with electromagnetic radiation at ω, which can be ionized with a single-photon transition from the upper state (Fig. 1). The evolution equations for the components of the density matrix for an exciting electric field of slowly varying amplitude $\mathcal{E}$ can be written[8]

$$i\dot{\sigma}_{12} = -\left[i\Delta\omega + \frac{1}{T_2} + \frac{\gamma_2}{2}\right] i\sigma_{12} - (\sigma_{22}-\sigma_{11})\mathcal{E}^2 , \tag{1}$$

$$\dot{\sigma}_{22}-\dot{\sigma}_{11} = 4\,\mathrm{Re}[\mathcal{E}^{*2}(i\sigma_{12})] - \gamma_2\sigma_{22} , \tag{2}$$

$$\dot{\sigma}_{11}+\dot{\sigma}_{22} = -\gamma_2\sigma_{22} , \tag{3}$$

where T_2 is the phase relaxation time and $\gamma_2 = 2\gamma\mathcal{E}^2$ the photoionization rate from the upper level 2, and $\Delta\omega = 2\omega - \omega_{12} - \delta\omega_{21}$ is the frequency detuning from resonance, including the Stark shift $\delta\omega_{12} = \alpha\mathcal{E}^2$. With the substitution $i\sigma_{12} = Q$, $(\sigma_{22}-\sigma_{11})/2 = W$, and $E^2 = 2\mathcal{E}^2$, and neglecting relaxation and ionization, the equations can be rewritten

$$\dot{Q} = -i\Delta\omega Q - WE^2 , \tag{4}$$

$$\dot{W} = \mathrm{Re}(E^{2*}Q) \tag{5}$$

with the initial condition $W(t=0) = -1$.

Equation (4) can be formally integrated, yielding

$$Qe^{i\Delta\omega t} = -\int_{-\infty}^{t} WE^2 e^{i\Delta\omega t'} dt' . \tag{6}$$

After a pulse has passed, $Q(t \gg \tau) = E_{2f}(\Omega)$, where $E_{2f}(\Omega)$ is the Fourier transform of $E^2(t)$. From the conservation relation $|Q|^2 + W^2 = 1$,

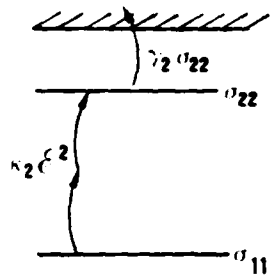

FIG. 1. Level diagram.

$$Q^2 = 1 - W^2 = -2W_0\Delta W = 2\Delta W , \tag{7}$$

where $\Delta W = W(t=\infty) - W(t=0)$. Combining Eqs. (6) and (7) gives the energy absorbed by the two-level system

$$2\Delta W = -|E_{2F}(\Delta\omega)|^2 . \tag{8}$$

The number of ions produced is simply the number of "lost atoms" $1-\sigma_{22}(t=\infty)-\sigma_{11}(t=\infty)$ in the system of Eqs. (1)–(3). The number of ions can also be estimated by integrating the ionization rate

$$N_{\text{ions}} = \int \gamma |E|^2 \sigma_{22} dt . \tag{9}$$

For small population transfers, $\sigma_{22} = \Delta W$ and

$$N_{\text{ions}} = \int \gamma |E|^2 \Delta W(t) dt . \tag{10}$$

Replacing ΔW by its average value $W(\infty)/2$,

$$N_{\text{ions}} \simeq \tfrac{1}{4}\gamma |E_{2F}(\Delta\omega)|^2 \theta , \tag{11}$$

where $\theta = \int_{-\infty}^{\infty} |E| dt$ is the "pulse area" or tipping angle of the pseudopolarization vector in the vector model of the two-photon resonant interaction.[9,10]

The expressions above hold in the approximation of weak excitation (θ small), no Stark shift (or any Stark shift but square pulse excitation). We see that both the absorption and the photoionization reflect the excitation spectrum. The photoionization spectrum is simply a fraction (proportional to the pulse area) of the Fourier spectrum of the Rabi frequency (which is, in this case, proportional to the square of the exciting electric field).

III. COHERENCE AND SPECTRAL CHARACTERISTICS

We will consider now more specifically the spectral characteristics (i.e., number of ions versus frequency) of an excitation mode of a sequence of pulses. In general, even if each individual pulse is pure in frequency (real amplitude function) the sequence of various pulses will be represented by a complex function E (because of the relative phase between pulses). A general property of the system of Eqs. (4) and (5) is that W—which determines in first approximation the photoionization—remains unchanged under a transformation $E \rightarrow E^*$, $\Delta\omega \rightarrow -\Delta\omega$ [indeed, under this transformation Eq. (4) is transformed in its complex conjugate and Eq. (5) remains unchanged]. This symmetry implies that the photoionization spectrum of a single unchirped pulse (E real) is symmetric. The symmetry is broken, however, in the case of a sequence of pulses with a phase difference $\Delta\phi$ different from 0 to π,

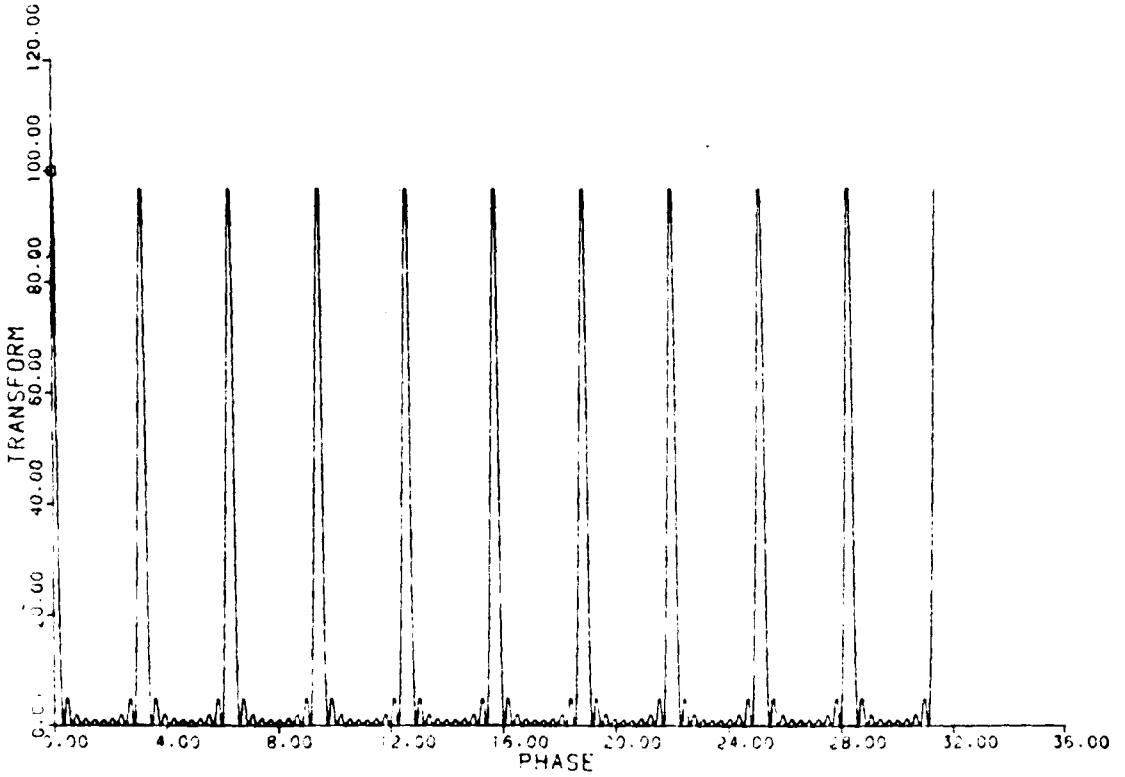

FIG. 2. Plot of the spectral intensity for a sequence of ten identical square pulses, as defined in Eq. (15).

that of the excitation pulses. In fact, the photoionization curves show all the characteristic features of a Fourier spectrum: the overall width is related to $1/\tau$, an increase of the phase difference between pulses shifts correspondingly the photoionization spectrum, and the width of the individual peaks in the photoionization spectrum decreases with increasing delay between pulses.

The Stark shift introduces an additional complexity by essentially creating a different resonance condition during and between pulses. This effect is demonstrated by the simple example of a sequence of two square pulses shown in Fig. 4. Increments of delay between the pulses by multiples of $2\pi/$(Stark shift) produce the same number of ions at resonance and at a detuning from resonance equal to the Stark shift. Departure from the simple approximations [Eqs. (6)–(10)] will be particularly significant for large-area pulses. "Photoionization spectroscopy" with a sequence of large-area pulses will enable a direct measurement of the photoionization rate from the upper state through the width of the individual peaks. Indeed, as shown in Fig. 5, the width of each peak in the photoionization spectrum is seen to increase with the transition rate to the continuum. It is interesting to note (Fig. 5) that the peak ionization is *smaller* for the higher ionization rate. The reduction in peak ionization rate is due to the increased dephasing associated with the transition rate to the continuum, resulting in a decrease in coherent excitation of the upper level.

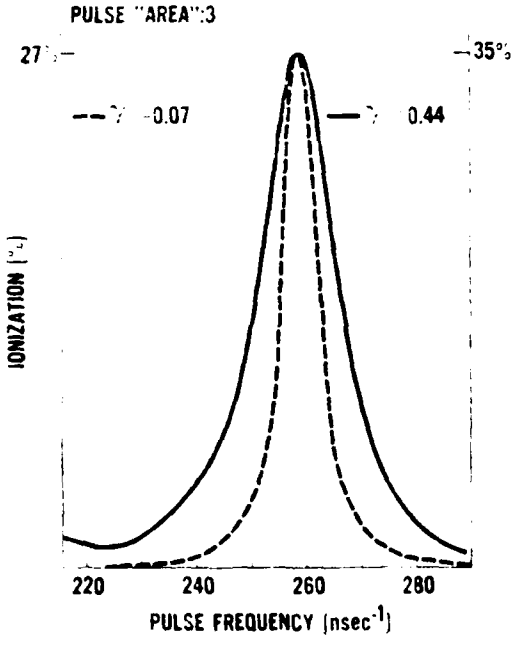

FIG. 5. Single peak of the ionization spectrum (% ions vs angular frequency in nsec^{-1}) for two different ionization rates. The exciting field consists of a sequence of ten Gaussian pulses, of 0.01 nsec duration (FWHM), and area $\theta = \int E^2 dt = 3$. The successive pulses are 0.4 out of phase. The medium parameters are the same as in the preceding figures, except for the ionization rates γE^2 being considered here. The scale to the right corresponds to the ionization rate of $0.07E^2$ (– – –), while the scale to the left pertains to the higher ionization rate of $0.44E^2$ (——).

V. IONIZATION BY A RANDOM PULSE SEQUENCE

An incoherent field can be described by a density matrix corresponding to an incoherent superposition of coherent states.[11] We choose to use for this superposition a series of identical pulses with a random distribution of delays and phases.

Under certain conditions a large number of experiments performed with a few pulses, for which the relative delays are distributed according, for instance, to a Poisson statistics, will have the same average result as the same experiment performed once with a very large number of pulses, distributed according to the same statistics. The average time between pulses has to be shorter than the coherence time of the particular resonance under investigation. We demonstrate next that, if the pulses are randomly distributed, the time evolution of the system driven by a sequence of identical pulses is proportional to the number of pulses and to the total fluence delivered, as expected for incoherent excitation. If, instead, the pulses are applied in phase and, for instance, in the condition of two-photon resonance, the absorption by the system is proportional to the *square* of the number of pulses. For demonstration purposes let us consider near two-photon resonance ($E^2 \gg \Delta\omega$) and weak pulses such that the approximation $W \simeq W_0$ can be made in Eq. (4). Each of the pulses of "area" $\Delta\theta = \int_{t_i}^{t_f} E^2 dt$ produces an increase in polarization

$$Q = W_0 \Delta\theta \exp(i\phi) . \tag{16}$$

If the pulses are all in phase (pulses equally spaced and in phase), $\Delta\theta$ is a constant angle, and after N pulses, $Q = N\Delta\theta$ and the energy absorbed W is proportional to the *square* of the number of pulses:

$$W = \frac{N^2 \Delta\theta^2}{2} . \tag{17}$$

If the distribution of pulse delays is random ($\Delta\omega\tau_d \ll 1$), then the phase in Eq. (1) is a random variable and the vector Q makes a random walk of N steps $\Delta\theta$ in the complex plane, starting from the origin. The resultant polarization is $Q = N\Delta\theta$, and the energy absorbed is proportional to the number of pulses:

$$W = N\frac{\Delta\theta^2}{2} . \tag{18}$$

It should be noted that by using a sequence of pulses we can compare coherent [as in Eq. (17)] versus incoherent [as in Eq. (18)] excitation, under the *same conditions of total fluence and peak intensity*. As expected, it is only in the case of incoherent excitation that the evolution of the system can be simply proportional to the total fluence delivered. The intensity dependence of the multiphoton process is not invoked in comparing the incoherent versus coherent case. The above considerations still hold in the more general case of a n-photon transition. The only difference is a generalized Rabi frequency in E^n. Equations (16)–(18) remain unchanged, with $\Delta\theta = \int_{t_i}^{t_f} E^n dt$. In the approximation $E^n \gg \Delta\omega$, and no intermediate level resonance, coherent excitation is characterized by an absorbed energy proportional to the *square* of the number of

pulses, while the absorption is directly proportional to the number of pulses in the incoherent case.

In order to study the influence of source coherence on the photoionization spectrum of lithium we calculated the number of ions as a function of pulse wavelength for a coherent and an incoherent sequence of ten pulses (Fig. 6). The "incoherent" curve (solid line, Fig. 6) corresponds to an average of 500 pulse sequences, each with a different set of relative delays taken from a Poisson distribution. The relative phases are uniform random numbers between 0 and 2π. The total area in each sequence of pulses is 1. As can be seen from Fig. 6, the photoionization from a coherent sequence (ten pulses equally spaced, relative phase $\pi/2$, dashed line in Fig. 6) can be much larger than that of the incoherent excitation. This result may appear to be in contradiction with experimental results of Lecompte *et al.*,[7] on the influence of coherence on multiphoton excitation. In the case of *nonresonant* N photon ionization of atoms reported in Ref. 6, the ionization probability is proportional to the Nth power of the laser intensity and therefore very sensitive to the transient intensity peaks that occur in a multimode laser pulse. The dependence of multiphoton ionization on laser coherence was studied by varying the number of oscillating laser cavity modes between one and one hundred. It has been estimated[7] that, in that case, a 20-mode laser is a good approximation of an incoherent source. The situation is more complex in the case of resonant multiphoton ionization as we are considering here. Indeed, the number of oscillating modes is varied by changing the bandwidth of the cavity. Therefore, the parameter coherence cannot be controlled independently of the resonance condition, since the spectral width of the laser source increases with decreasing coherence. In the approach used here, however, the laser coherence is modified *at constant bandwidth*, since the spectrum of the pulse sequence is contained within the spectrum of a single pulse.

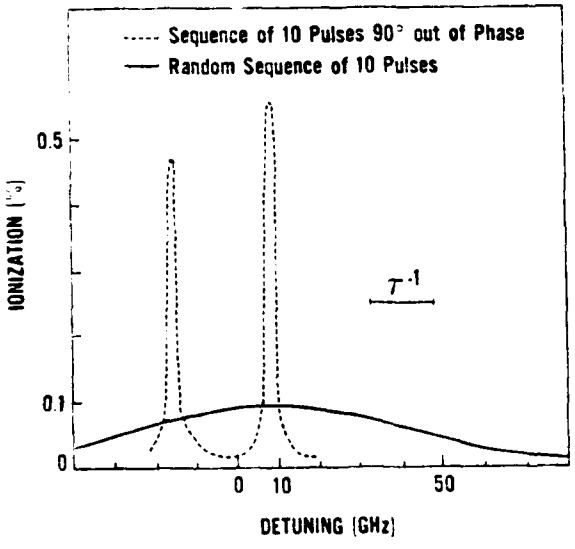

FIG. 6. Ionization vs angular frequency (nsec^{-1}) for a sequence of ten pulses. Each pulse is Gaussian shaped of area 0.1. The solid line corresponds to a random pulse sequence, the dashed line to a sequence of equally spaced (0.09 nsec) pulses, each 90° out of phase with the former. Each pulse of the sequence is Gaussian, with a duration of 0.01 nsec (FWHM). The statistical result (——) is obtained by taking the average of 500 "excitations," each with a sequence of pulses distributed (in relative delay) according to a Poisson distribution. The relative phases between pulses are taken to be random numbers between 0 and 2π. The medium parameters are the same as for Fig. 2. The average delay between pulses is 0.09 nsec.

It is interesting to note that in a recent experimental study of four-photon (three-photon resonant) ionization of caesium atoms, Lompre *et al.*[7] found also an increase in the width of the spectral dependence of the ionization for incoherent versus coherent excitation. The hyperfine structure of the resonance is still observed in coherent excitation, while it is not in the incoherent case (Ref. 7, Fig. 8). However, in that particular experiment[7] the coherence was varied by changing the number of modes of the laser and comparing data for the same *average intensity*. Therefore, temporal fluctuations make the *peak intensity* highest in the incoherent case, resulting in a higher ionization in the incoherent case than in the coherent case. In an experiment in which the coherence is varied by varying the temporal distribution of identical pulses, as suggested here, the peak intensity as well as the spectral bandwidth remain constant, while the coherence is modified within the pulse spectrum.

Photon statistics. Let us consider a limiting case where each pulse of the sequence contains only one photon. The "pulse sequence statistics" is then nothing more than the photon statistics of the radiation field. The number of pulses N is now the number of photons in the excitation, each of these photons $\hbar\omega$ driving coherently an n-photon resonant system (i.e., a two-level system of energy $n\hbar\omega$). For instance, in the simple argument at the beginning of this section, the elementary increment of the n-photon off-diagonal element becomes

$$\Delta\theta = \int_{t_i}^{t_f} E^n dt = \eta(\hbar\omega)^{n/2} , \tag{19}$$

η being a proportionality coefficient.

It should be noted that the photon energy does not appear explicitly in any calculations carried out in the slowly varying envelope approximation (SVEA). The statistical sequence of identical macroscopic coherent pulses (each of them being a coherent superposition of M photons) interacting with the n-photon resonant atoms is identical (within the SVEA) to a "photon statistics" in a fictitious world where Planck's constant is $M\hbar$. The transition frequency at $\omega_0 = n\omega$ is in the condition of n-photon resonance with each pulse $(M\hbar)\omega_0 = n(M\hbar\omega)$. Since Planck's constant appears only implicitly (in the scaling of the generalized Rabi frequency E) in the theoretical model, all the equations of the theoretical model remain unchanged by the "transformation." The elementary increment of the off-diagonal element for the standard pulse of the train can also be expressed in terms of the "pseudophoton" energy $(M\hbar)\omega$, in a similar way as in Eq. (19):

$$\Delta\theta = \int E^n dt = \eta[(M\hbar)\omega]^{n/2} . \tag{20}$$

This similitude offers an intuitive justification for the use of a pulse sequence to study the statistical response of a

multiphoton resonant system. We are essentially creating a "pseudophoton statistics." This concept is legitimized because Planck's constant does not appear explicitly in this formalism (i.e., the photon energy is still small compared with the total excitation energy). Since the model of the pseudostatistics concept is equivalent to the theoretical model used in Sec. III, it does not bring any new light to the problem. However, it offers a convenient interpretation to the approach that is being taken here, to study coherence effects through the use of pulse sequences.

VI. EXPERIMENTAL CONSIDERATIONS

In this section we briefly discuss the experimental implementation of the excitation scheme discussed above. The use of a Mach Zehnder interferometer to generate two-pulse sequences has been demonstrated in a study of two-photon resonant coherent propagation in lithium vapor.[13,14] Optical delays adjusted with interferometric accuracy were used to control the relative phase and delay between pulses. A He-Ne laser was sent through the same Mach Zehnder interferometer to monitor the optical delays (hence the phases) with subwavelength accuracy. A series of optical delay lines can generate multiple-pulse sequences. Instead of Mach Zehnder interferometers a cascade of N optical delay lines as sketched in Fig. 7 can be used to generate a $3N$-pulse sequence. For a beam-splitter reflectivity of $R=68\%$, each "module" of Fig. 7 produces a series of three identical pulses, each carrying 22% of the input pulse energy.

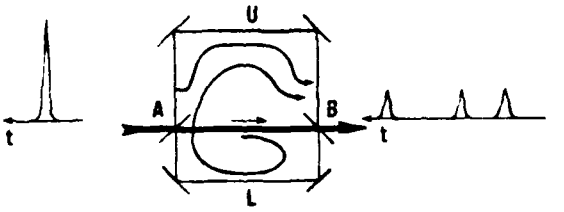

FIG. 7. Sketch of an interferometric delay line to split an input pulse into a sequence of three identical pulses. If the beam splitters A and B have, respectively, a reflection coefficient of 0.68 and 0.32, the successive pulses follow the paths AB, AUB, and $ABLAUB$ and each carries 22% of the original beam.

The shorter the wavelength, the more difficult it is to control the relative phase of pulses with optical delay lines. As noted earlier, the approach proposed here applies also to multiphoton dissociation of molecules involving, for instance, the use of picosecond CO_2 lasers,[15] for which coherent pulse sequencing (i.e., pulse sequencing while maintaining the relative phases) would be particularly easy.

ACKNOWLEDGMENTS

The work was supported by the Air Force Office of Scientific Research (AFOSR) under Grant No. 820332, The Robert A. Welch Foundation, and the National Science Foundation under Grants Nos. Nb ECS-8406985 and CHE-8203966.

[1] A. Villaeys and K. F. Freed, Chem. Phys. **13**, 271 (1976).
[2] W. S. Warren, D. P. Weitekamp, and A. Pines, J. Chem. Phys. **73**, 2084 (1980); W. S. Warren and A. H. Zewail, J. Chem. Phys. **78**, 2279 (1983); **78**, 2298 (1983).
[3] J.-C. Diels, J. Stone, S. Besnainou, M. F. Goodman, and E. Thiele, Opt. Comm. **37**, 11 (1981); S. Besnainou, J.-C. Diels, and J. Stone, J. Chem. Phys. **81**, 143 (1984).
[4] M. F. Goodman, J. Stone, and E. Thiele, J. Chem. Phys. **63**, 2929 (1975).
[5] J. Stone and M. F. Goodman, J. Chem. Phys. **71**, 408 (1979) and references contained therein.
[6] C. Lecompte, G. Mainfray, C. Manus, and F. Sanchez, Phys. Rev. A **11**, 1009 (1975).
[7] L.-A. Lompre, G. Mainfray, C. Manus, and J. P. Marinier, J. Phys. B **14**, 4307 (1981).
[8] J.-C. Diels and A. T. Georges, Phys. Rev. A **19**, 1589 (1979).
[9] J.-C. Diels, Opt. Quantum Electron. **8**, 513 (1976).
[10] D. Grischkowsky, M. M. T. Loy, and P. F. Liao, Phys. Rev. A **12**, 2514 (1975).
[11] R. J. Glauber, Phys. Rev. **131**, 2766 (1963).
[12] J.-L. De Bethune, Nuovo Cimento B **12**, 101 (1972).
[13] H. Vanherzeele, H. J. Mackey, and J.-C. Diels, Appl. Opt. **23**, 2056 (1984).
[14] J.-C. Diels and H. Vanherzeele, in *Proceedings of the Topical Meeting on Ultrafast Phenomena, Monterey, California, 1984* (Springer, Berlin, 1984), p. 233.
[15] P. B. Corkum, Opt. Lett. **8**, 515 (1983).

END

DTIC

7-86